creative commons
COMMONS DEED

저작자표시-비영리-변경금지 2.0 대한민국

이용자는 아래의 조건을 따르는 경우에 한하여 자유롭게

- 이 저작물을 복제, 배포, 전송, 전시, 공연 및 방송할 수 있습니다.

다음과 같은 조건을 따라야 합니다:

저작자표시. 귀하는 원저작자를 표시하여야 합니다.

비영리. 귀하는 이 저작물을 영리 목적으로 이용할 수 없습니다.

변경금지. 귀하는 이 저작물을 개작, 변형 또는 가공할 수 없습니다.

- 귀하는, 이 저작물의 재이용이나 배포의 경우, 이 저작물에 적용된 이용허락조건을 명확하게 나타내어야 합니다.
- 저작권자로부터 별도의 허가를 받으면 이러한 조건들은 적용되지 않습니다.

저작권법에 따른 이용자의 권리는 위의 내용에 의하여 영향을 받지 않습니다.

이것은 이용허락규약(Legal Code)을 이해하기 쉽게 요약한 것입니다.

Disclaimer

dCollection

[Synthesis and Characterization of Novel Photoactive Materials for Polymer Solar Cells]

[Boram Kim]

[Interdisciplinary School of Green Energy]

Graduate School of UNIST

[Synthesis and Characterization of Novel Photoactive Materials for Polymer Solar Cells]

A thesis
submitted to the Interdisciplinary Department of Energy Engineering
and the Graduate School of UNIST
in partial fulfillment of the
requirements for the degree of
[Master of Science]

[Boram Kim]

6. 27. 2013
Approved by

Major Advisor
[Changduk, Yang]

[Synthesis and Characterization of Novel Photoactive Materials for Polymer Solar Cells]

[Boram Kim]

This certifies that the thesis of [Boram Kim] is approved.

6. 27. 2013

[signature]

Thesis supervisor: [Changduk, Yang]

[signature]

[Jin Young, Kim]

[signature]

[Yongseok, Jun]

Abstract

The most widely used configuration of polymer solar cells is the so called “bulk hetero-junction” device in which the active layer consists of a blend of an electron-donating materials, e.g., a *p*-type conjugated polymers, and an electron-accepting material such as [6,6]-phenyl C_{61}-butyric acid methyl ester. Several factors are important in further improving the efficiency of a PSC. Among these, the development of an electron-donating polymer has with low band gap to efficiently absorb light in the visible area of the solar spectrum and structural manipulation of the acceptor component, to optimize the solar cell performance. Therefore, there is still plenty of room to tune the efficiencies of BHJ photovoltaic cells. The main topics of this work are the synthesis of novel donating polymers and electron acceptors like fullerenes and their application in BHJ PSCs. Firstly, poly[*N*-9′-heptadecanyl-2,7-carbazole-*alt*-5,5-(4′,7′-di-2-selenienyl-2,1,3-benzothiadiazole)] (**PCDSeBT**), in which diselenienylbenzothiadiazole (DSeBT) monomer alternately flanks with 2,7-carbazole unit is synthesized for a low band gap polymer to harvest more solar photons. Besides, the photovoltaic properties of **PCDSeBT** in typical BHJ devices with PCBM are investigated. This work has already been published in Macromolecules. Secondly, *N*-9′-Heptadecanyldithieno[2,3-*b*;7,6-*b*]carbazole-based polymers (**PTCZTBT**, **PTCZTfBT**, **PTCZTffBT, PTCZTTT**, **PTCZTPT**, **PTCZTQ**, **PTCZTfQ, PTCZTffQ),** respectively, comprising a S- and N-containing heteroarene are prepared for potential usage in efficient PSCs. In the last part, considering possible combined effects from the 56 π-electron system by the bisadduct framework and the increased light absorption in the visible region by the additional chromophores, we report the synthesis and characterization of **bis-PCBM dyad** containing 4-nitro-α-cyanostilbene units for usage in efficient PSCs. This work has already been published in Tetrahedron.

Contents

List of figures

Figure 12. *J-V* characteristics measured by the space charge limited current (SCLC) method with **PCDSeBT**:$PC_{71}BM$ (1:4 w/w) films under dark conditions before and after thermal annealing for hole-only device (a) and electron-only device (b).

Figure 13. UV-Vis absorption spectra of **TCZT's polymers** in $CHCl_3$ (a) and the thin film on the quartz (b).

Figure 14. Rational design motif of **bis-PCBM dyad**; 4-Nitro-α-cyanostilbene was chosen as additional light-harvesting unit to provide a higher J_{sc}. In principle, the LUMO can be raised by bis-adduct framework due to 56 π-electron system.

Figure 15. ^1H NMR (a) of **10** and ^1H and ^{13}C NMR (b, c) spectra of **bis-PCBM dyad** in $CDCl_3$. The digital photographs of **10** and **bis-PCBM dyad**.

Figure 16. UV−Vis absorption of **10**, PCBM, bis-PCBM, and **bis-PCBM dyad** in $CHCl_3$ solution.

Figure 17. Cyclic voltammograms of PCBM and **bis-PCBM dyad** in *o*-DCB solution. Experimental conditions: values for $(E_{pa} + E_{pc})/2$ in V versus Fc/Fc^+; 10^{-4}–10^{-3} mol/L *o*-DCB solution; Bu_4NClO_4 (0.1 M) as supporting electrolyte; Pt wire as counter electrode; 50 mV/s scan rate.

Figure 18. *J-V* characteristics of **bis-PCBM dyad** of conventional (a) and the inverted (b) devices under illumination of AM 1.5G, 100 mW/cm^2. Inset is a schematic of the device architectures of (a) and (b), respectively.

List of tables

List of Schemes

Nomenclature

BHJ PSCs	Bulk-heterojunction polymer solar cells
FET	Field-effect transistors.
XRD	X-ray diffraction analysis
SCLC	Space charge-limited current (SCLC) model
bis-PCBA	Bis-[6,6]-phenyl C_{61}-butyric acid
DSeBT	Di(2′-selenienyl)-2,1,3-benzothiadiazole
PCDSeBT	Poly[*N*-9′-heptadecanyl-2,7-carbazole-*alt*-5,5-(4′,7′-di-2-selenienyl-2,1,3-benzothiadiazole)]
PCDTBT	Poly[*N*-9′-heptadecanyl-2,7-carbazole-*alt*-5,5-(4′,7′-di-2-thiophenyl-2,1,3-benzothiadiazole)]
TCZT	*N*-9′-Heptadecanyl-3,8-bis(trimethylstannyl)dithieno[2,3-*b*;7,6-*b*]carbazole
PTCZTBT	Poly[*N*-9′-heptadecanyldithieno(2,3-*b*;7,6-*b*)carbazole-*alt*-(2,1,3-benzothiadiazole)]
PTCZTfBT	Poly[*N*-9′-heptadecanyldithieno(2,3-*b*;7,6-*b*)carbazole-*alt*-4,7-(5-fluoro-2,1,3 benzothiadiazole)]
PTCZTffBT	Poly[*N*-9′-heptadecanyldithieno(2,3-*b*;7,6-*b*)carbazole-*alt*-4,7-(5,6-difluoro-2,1,3-benzothiadiazole)]
PTCZTTT	Poly[*N*-9′-heptadecanyldithieno(2,3-*b*;7,6-*b*)carbazole-*alt*-4,6-(1-prophanone,1-thieno[3,4-*b*]thiophene)]
PTCZTPT	Poly[*N*-9′-heptadecanyldithieno(2,3-*b*;7,6-*b*)carbazole-*alt*-1,3-(5 octylthieno[3,4]pyrrol-4,6-dione)]
PTCZTQ	Poly[*N*-9′-heptadecanyldithieno(2,3-*b*;7,6-*b*)carbazole-*alt*-5,8-(2,3-bis(octyloxy)phenylquinoxaline]
PTCZTfQ	Poly[*N*-9′-heptadecanyldithieno(2,3-*b*;7,6-*b*)carbazole-*alt*-5,8-(6-fluoro-2,3-bis(octyloxy)phenylquinoxaline]
PTCZTffQ	Poly[*N*-9′-heptadecanyldithieno(2,3-*b*;7,6-*b*)carbazole-*alt*-5,8-(6,7-difluoro-2,3-bis(octyloxy)phenylquinoxaline]
$Pd_2(dba)_3$	Tris(dibenzylideneacetone)dipalladium
$Pd(PPh_3)_2Cl_2$	Bis(triphenylphosphine)palladium(II) dichloride
P(*o*-Tol)$_3$	Tri-*o*-tolylposphin
Bu_4NClO_4	Tetrabutylammonium perchlorate
***n*-Bu_4NPF_6**	Tetra-*n*-butylammonium hexafluorophosphate
$AgNO_3$	Silver nitrate
$MgSO_4$	Magnesium sulfate
$NaHSO_4$	Sodium bisulfate
$NaHCO_3$	Sodium bicarbonate
$Na2S{\cdot}9H_2O$	sodium sulfide nonahydrate
K_3PO_4	Potassium phosphate
KI	Potassium iodide
KIO_3	Potassium iodate
KOH	Potassium hydroxide
HCl	Hydrochloric acid
THF	Tetrahydrofuran
***o*-DCB**	*ortho*-Dichlorobenzene

EtOH	Ethanol
MeOH	Methanol
DMF	*N,N*-Dimethylformamide
CH_2Cl_2	Dichloromethane
AcOH	Acetic acid
Et_3N	Triethylamine
NMP	1-Methyl-2-pyrrolidinone
Et_2O	Diethyl ether
DMSO	Dimethyl sulfoxide

Ⅰ. Introduction

1.1 Background and General Concept of Polymer Solar Cells

Generally, Solar cells have been made from inorganic materials like silicon. Though these solar cells have high efficiency, they are very expensive and heavy. Due to the shortage of silicon supply, the interest about the solar cells made of organic material has been increasing. The main reason for the extensive interest in organic semiconducting materials is their potential for the realization of a low cost, easily processed and flexible renewable energy source. Since R.H Friend et al. introduced poly phenylene vinylene (PPV) as a photoactive donor material to the polymer solar cell for the first time, bilayer device structure consisting of polymer donor and fullerene acceptor had been utilized in the initial stage.[1] Figure 1 shows scheme of basic processes occurring in polymer solar cells. The light-generated electrons are transferred to low work function metals and the holes are transferred to ITO due to its high work function.

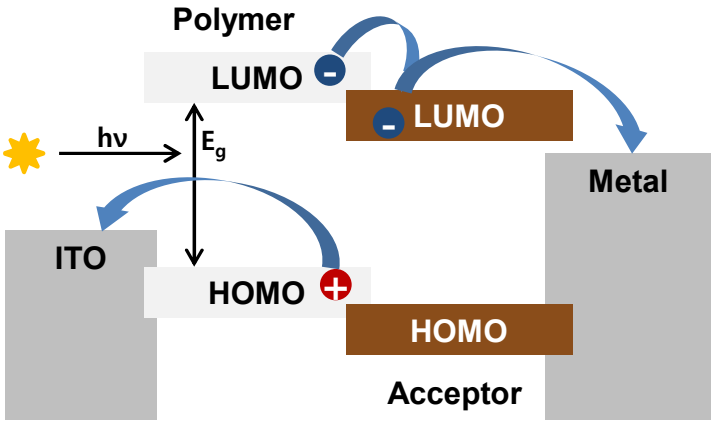

Figure. 1. Scheme of basic processes occurring in polymer solar cells.

The core materials of polymer solar cell composition, conjugated polymers are composed of loosely tied π-bond relative to strong σ-bond. Like this the delocalized materials absorb the light, generating the photo-generated charge carriers. It takes only 100 picoseconds for recombination of the electron-hole pair so the exciton diffusion length is approximately known as 10 nm. To generate electrons and holes after breaking the light generated exciton without recombination, p-n junction interfaces should be within 10 nm from the exciton generation. Since the thickness of bilayer hetero-junction devices is generally about 100nm, most of excitons cause recombination. Therefore, they had greatly a limitation of the performance by the small area of charge-generating interface between the donor and acceptor (Figure 2a). As an efficient strategy towards the increase of interfacial area between donor and acceptor, bulk hetero-junction (BHJ) device structure was developed by introducing the blend of

donor and acceptor as the active layer. Therefore, excitons generated by solar light can effectively be separated into holes and electrons (Figure. 2b). Heeger group[2] proved this point through using film of PPV derivative which shows fluorescence and C_{60}. The film was shown that the fluorescence was drastically reduced when two compounds were blended.

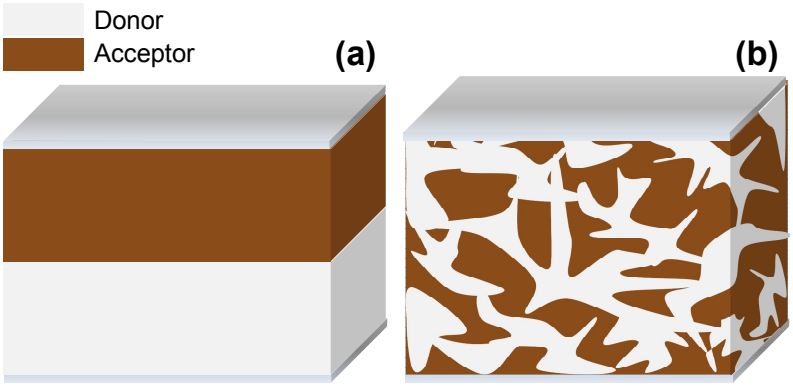

Figure. 2. Two different structures of hetero-junctions, phase separated bilayer (a) and bulk hetero-junction (b).

1.2 Synthesis of Conjugated Polymers for Bulk Hetero-Junction Polymer Solar Cells

One of the most important methods for preparation of conjugated polymers is chemical polycondensation. The Ni promoted coupling reactions (Yamamoto coupling[3], Kumada coupling[4], Negishi coupling[5]), Palladium catalyzed reactions (Heck coupling[6], Suzuki coupling[7], Stille coupling[8], Sonogashira coupling[9], Buchwald-Hartwig coupling, Kumuda coupling[4], Negishi coupling[5], Hiyama coupling[10]), Cu-catalyzed reactions (Ullmann Reaction[11], Glaser coupling[12]) and coupling reactions not involving metal catalysis (Wittig coupling[13], Knoevenagel coupling[14]) were applied. Up to now, the palladium catalyzed polycondensations were regarded as the best methods. Especially Suzuki coupling and Stille coupling are widely used in BHJ polymer solar cells (PSCs). The Stille is the reaction between organostannanes and organohalide compounds (Scheme 1).

$$\text{R-X + R'SnR''}_3 \xrightarrow{\text{Pd}} \text{R-R'}$$

Scheme 1. Scheme of Stille coupling.

Advantages of Stille reaction is stereospecific, regioselective, and typically gives excellent yields. Organotin and organohalide compounds can be conveniently prepared, typically without the requirement for protecting functionalities present in the monomers, and are far less oxygen- and moisture-sensitive than many of their other organometallic counterparts, e.g., Grignard reagents, organolithium reagents, and others. With its mild reaction conditions, high monomer solubility, tolerance for a wide range of functional groups, and facile preparation of monomers, the Stille reaction represents one of the most versatile protocols in the arsenal of organometallic chemistry. The general mechanism of the Stille reaction is shown in Figure 3. The active catalyst is believed to be a 14-electron palladium (0) complex, which can be generated from a suitable palladium (0) precursor such as $Pd_2(dba)_3$ and $Pd(PPh_3)_4$. Palladium (0) complexes are nucleophilic and they react readily with organic electrophiles in an oxidative addition reaction to produce a 16-electron palladium (II) intermediate $RPdL_2X$. The electrophilic component RX in the reaction is frequently an organohalide or organotriflate compound. The next step occurring in the catalytic cycle of the Stille reaction is a transmetallation reaction. In the transmetallation step, one group from the organotin reagent transfers to the palladium (II) intermediate whilst the halide or triflate group becomes associated with the tin of the organostannane. Fortunately, alkyl groups migrate from tin to palladium at the slowest rate. Mixed organostannanes that contain three spectator methyl or butyl groups can therefore be used so that exclusive transfer of a more chemically complex group such as a vinyl or aryl moiety can occur. The transmetallation step is the rate determining step in the catalytic cycle. In the final step of the catalytic cycle the cross-coupled product is expelled from the palladium (II) intermediate and the active

palladium (0) catalyst is regenerated.

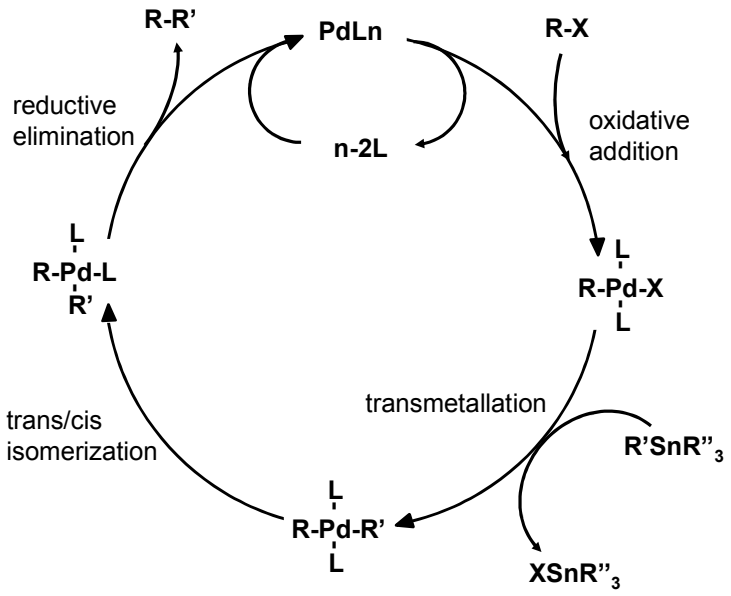

Figure 3. Mechanism of Stille coupling.

The Suzuki coupling is the reaction between organoboron compounds and organohalide compounds (Scheme 2).

$$\mathrm{Ar\text{-}X + Ar'B(OH)_2 \xrightarrow[base]{Pd} Ar\text{-}Ar'}$$

Scheme 2. Scheme of Suzuki coupling.

Potassium trifluoroborates and organoboranes or boronic esters may be used in place of boronic acids. One difference between the Suzuki mechanism and that of Stille coupling is that the boronic acid must be activated, generally with a base. This activation of the boron atom enhances the polarization of the organic ligand, and facilitates transmetallation. The general mechanism of Suzuki reaction is shown in Figure 4. The first step is the oxidative addition of palladium to the halide to form the organo-palladium species. This species reacts with a base to give intermediate Ar-Pd (II)-OH, which via transmetallation with the boronate complex forms the organopalladium species Ar-Pd (II)-Ar'. Reductive elimination of the desired product restores the original palladium catalyst.

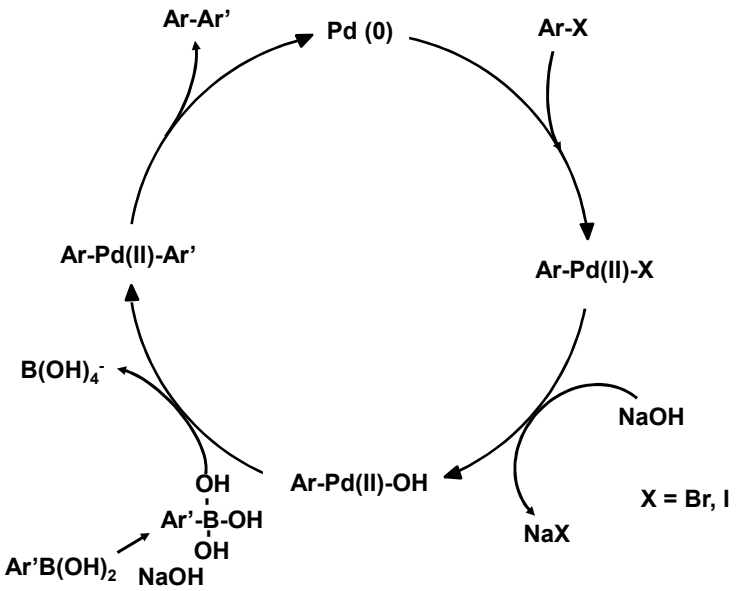

Figure 4. Mechanism of Suzuki coupling.

1.3 Fullerene derivatives for Bulk Hetero-Junction Polymer Solar Cells

In the autumn of 1985, Robert F. Curl, Harold W. Kroto and Richard E. Smalley discovered a new carbon of very stable spheres, and won The Nobel prize in Chemistry 1996. The covalent binding of fullerene to electro active donor molecules such as porphyrins allows for the development of molecular dyads in which photoinduced energy- and/or electron transfer takes place. In many of such architectures C_{60} accelerates photoinduced charge separation and retards charge recombination in the dark. As a consequence, long-lived charge separated states can be generated, which can be used for subsequent energy conversion processes. The electron-accepting ability of C_{60} is its most characteristic chemical property. In 1990, the electron affinity of C_{60} was soon found to translate into the solution phase. Therefore C_{60} was selected as the electron acceptor for bilayer PSCs by Sariciftci et al. in 1992.[15] However, the performance of bilayer PSCs is low because of its short diffusion length of the exitons. To solve this problem, BHJ devices structure using PPV as donor materials and C_{60} as acceptor materials were developed. Yet, the performance of BHJ PSCs of PPV and C_{60} have been restricted due to that concentration of C_{60} could not increase owing to the tendency to crystallize and the poor solubility of C_{60} in organic solvents hinder direct applications in inexpensive solution-based processing techniques unless the bare C_{60} structure.[16] To overcome this difficulty, many researchers have studied soluble C_{60} derivatives. In 1995, one particular solubilizing derivative synthesized by Wudl and Hummelen, namely, [6,6]-phenyl-C_{61}-butyric acid methyl ester (PCBM), which dramatically increased the power conversion efficiency (PCE) of early PSCs by enabling the fullerene component to be co-soluble with the *p*-type conjugated polymers.[17] After that, Much of the research efforts towards new fullerene derivatives has been devoted to modifying the substituents of PCBM by introducing additional substituents on its phenyl ring,[17c, 18] or replacing the phenyl ring with other groups,[19] since the electronic properties of PCBM derivatives can be altered by the interaction between the aromatic substituent and the fullerene cage which occur through 'periconjugation'.[20]

1.2 Motivation of the Work

For high performance PSCs, many researchers have studied novel donor and acceptor materials. Poly(2,7-carbazole-alt-dithienylbenzothiadiazole) (PCDTBT) is one excellent donor material which has high PCE, but it has larger band gap compared with the proposed 1.5−1.7 eV of the ideal band gap for PCE exceeding 10%. Therefore, in order to reduce band gap of PCDTBT, we have replaced thiophene of PCDTBT with selenophene which has the individual effects of the smaller ionization potential (IP) and almost the same electronegativity of selenium relative to sulfur atom.

Also, some fused aromatic polymers such as S-containing heteroarene are shown high mobilities with srong π-π interation, so, to improve the mobilities, a lot of donor polymers were attempt to introducing fused thiophene units in the polymer backbone. However, with the increase of the size of the S-containing heteroarene, density of the alkyl chains along the polymers chain decreases, which may result in the low solubility of the polymers. For improving solubility, we have synthesized dithieno[2,3-*b*;7,6-*b*]carbazole. Carbazole which has nitrogen atom can allow introducing more alkyl chains into the polymer.

Finally, we synthesized bis-PCBM dyad containing 4-nitro-α-cyanostilbene units for usage in efficient PSCs, because the replacement of the ester methyl group of PCBM with 4-nitro-α-cyanostilbene was shown increasing the absorption, enhancing the solubility, and suppressing the crystallization. We expected high performance of bis-PCBM dyad based on devices with increasing chromophores.

Chapter II. A Selenophene Analogue of PCDTBT: Selective Fine-Tuning of LUMO to Lower of the Bandgap for Efficient Polymer Solar Cells

In this chapter, In an attempt to further improve the performance of the PCDTBT-based polymer solar cells (PSCs), we have synthesized a selenophene analogue of PCDTBT, namely, **PCDSeBT**, in which diselenienylbenzothiadiazole (DSeBT) monomer alternately flanks with a 2,7-carbazole unit. The intrinsic properties of **PCDSeBT** are not only characterized by UV−Vis absorption, cyclic voltammetry (CV), and organic field-effect transistors (OFETs) but also the surface morphology, mobilities of space charge-limited current (SCLC) model, and polymer solar cells (PSCs) in its bulkheterojunction (BHJ) active layer with [6,6]-phenyl C_{71}-butyric acid methyl ester ($PC_{71}BM$) are evaluated in detail. It is found that **PCDSeBT** simultaneously has a low-lying highest occupied molecular orbital (HOMO) energy level at −5.4 eV and a low bandgap of 1.70 eV as required by the ideal polymers for BHJ PSCs. The high current of 11.7 mA/cm^2 is obtained for **PCDSeBT**-based PSCs, to our knowledge, which is among the highest short-circuit current density (J_{SC}) values obtained from a BHJ device consisting of PCDTBT derivatives and [6,6]-phenylC61-butyric acid methyl ester (PCBM). The high J_{SC} value, along with a moderate fill factor (FF) of 45% and a high open-circuit voltage (V_{OC}) of 0.79 V, yields a power conversion efficiency (PCE) of 4.12%, which is about 37% increase in PCE from a PCDTBT-based reference device. On the basis of our results, one can be concluded that the DSeBT placement for construction of donor (D)-acceptor (A) polymers is an easy and effective way to realize both the higher J_{SC} and V_{OC} values in PSCs, as a consequence of the selective lower-lying lowest unoccupied molecular orbital (LUMO) with the HOMO being almost unchanged, together with the effective broadening on the absorption band.

2.1 Introduction

With deep understanding of efficient photoinduced electron transfer within an interpenetrating network by simple blending π-conjugated polymers (electron donor) with fullerene derivatives (electron acceptor),[15] bulk hetero-junction (BHJ) polymer solar cells (PSCs) based on poly(3-hexylthiophene) (P3HT):[6,6]-phenyl C_{61}-butyric acid methyl ester (PCBM) have been extensively investigated, leading to great progress in power conversion efficiencies (PCEs) of 4−5%.[17b, 21] Yet, the PCE of P3HT-based PSCs is limited by its relatively large band gap (~1.9 eV) with major loss of the solar radiation as well as low open circuit-voltage (V_{OC} ≅ 0.6 V) due to the relatively small energy difference between the highest occupied molecular orbital (HOMO) of P3HT and the lowest unoccupied molecular orbital (LUMO) of PCBM. By taking into consideration using low band gap polymers to harvest more solar photons, researchers have devoted much effort recently to reducing the band gap of polymers. This approach has provided a remarkable short-circuit current density (J_{SC}) of 16 mA/cm^2,[22] whereas, in general, the V_{OC} has suffered[23] because of a higher than the HOMO optimal energy level in order to pursue a lower band gap. In the PSCs community, poly(2,7-carbazole-altdithienylbenzothiadiazole) (PCDTBT) is one excellent example for a low HOMO (−5.45 eV) as required by the 'ideal' π- conjugated polymers, which led to a high V_{OC} value over 0.8 V and outstanding stability against oxidation at high temperatures.[24] The initial PCE reached 3.6%[24a] in a typical BHJ device and has been subsequently improved to exceeding 6% by BHJ layer thickness optimization and nanomorphology control using mixed solvent mixtures.[25] However, the band gap of PCDTBT is still relatively larger than the proposed 1.5−1.7 eV of the ideal polymers for PCEs exceeding 10%. Recently, to further lower the band gap of PCDTBT without sacrificing its high V_{OC}, Hsu et al.[26] and our group[17a] independently reported PCDTBT-based ladder-type polymers with forced planarity of which device performance showed impressive PCEs of up to 4.59% with reduced band gap (ca. 0.2 eV) in comparison with that of PCDTBT. However, the multiple synthetic steps for the ladder-type PCDTBTs have restricted the realization for their usage in BHJ devices. Herein, we present an easily obtainable selenophene analogue of PCDTBT, namely, poly(2,7-carbazole-alt-diselenienylbenzothiadiazole) (**PCDSeBT**) by replacing thiophenes with selenophene rings in the polymer backbone. Such a structural modification would be expected the lower-lying LUMO with the HOMO being largely unaffected due to the individual effects of the smaller ionization potential (IP) and almost the same electronegativity of selenium relative to sulfur atom.[27] In addition, interchain-charge transfer should be facilitated by intermolecular Se···Se contacts, most likely leading to a widen absorption band and enhanced mobility that are desirable for high photocurrents.[28] Our preliminary investigation on the photovoltaic properties of **PCDSeBT** in typical BHJ devices with [6,6]-phenyl C_{71}-butyric acid methyl ester ($PC_{71}BM$) shows a highly respectable PCE of 4.12% on account of the high J_{SC} and V_{OC}.

2.2 Results & Discussion

2.2.1 Synthesis

The synthetic routes to the monomers (**M1** and **M2**) and **PCDSeBT** are shown in Scheme 3. Compounds **1**, **2**, **3**, and **4** were synthesized according to the previously reported procedures.[24a, 29] The diboronic ester monomer **M1** was easily synthesized from precursor **3**, by dilithiation at −78 °C, followed by quenching with 2-iso-propoxy-4,4,5,5-tetrametyl-1,3,2-dioxaborolane in anhydrous THF in a yield of 79%. As the key building block selenium-containing heterocyclic intermediate di(2′-selenienyl)-2,1,3-benzothiadiazole (DSeBT) **6**[29] was prepared by Pd-catalyzed Stille coupling reaction of dibromobenzothiadiazole **4** and monostannylselenophene **5**, which was then dibrominated by N-bromosuccinimide (NBS) to yield comonomer **M2** (2 steps, 52% overall yield). The target poly(2,7-carbazole-alt-diselenienylbenzothiadiazole) (**PCDSeBT**) was obtained by Suzuki polymerization of **M1** and **M2** in degassed toluene/water with K_3PO_4 as an organic base, $Pd_2(dba)_3$ as a catalyst, and P(*o*-tol)$_3$ as the corresponding ligand at 90 °C for 3 days. The crude polymer was purified by reprecipitation and Soxhlet extraction with methanol, acetone, hexane, and chlorobenzene. Details of synthesis of monomers, polymerization, and their characterizations are given in the Experimental Section. After purification, gel-permeation chromatography (GPC) analysis against PS standard exhibits a number-averaged molecular mass (M_n) of 83 000 g/mol with a polydispersity (PDI) of 2.51. The polymer is readily soluble in common solvents such as chloroform, toluene, THF, and chlorobenzene.

Scheme 3. Synthetic route to **PCDSeBT**[a].

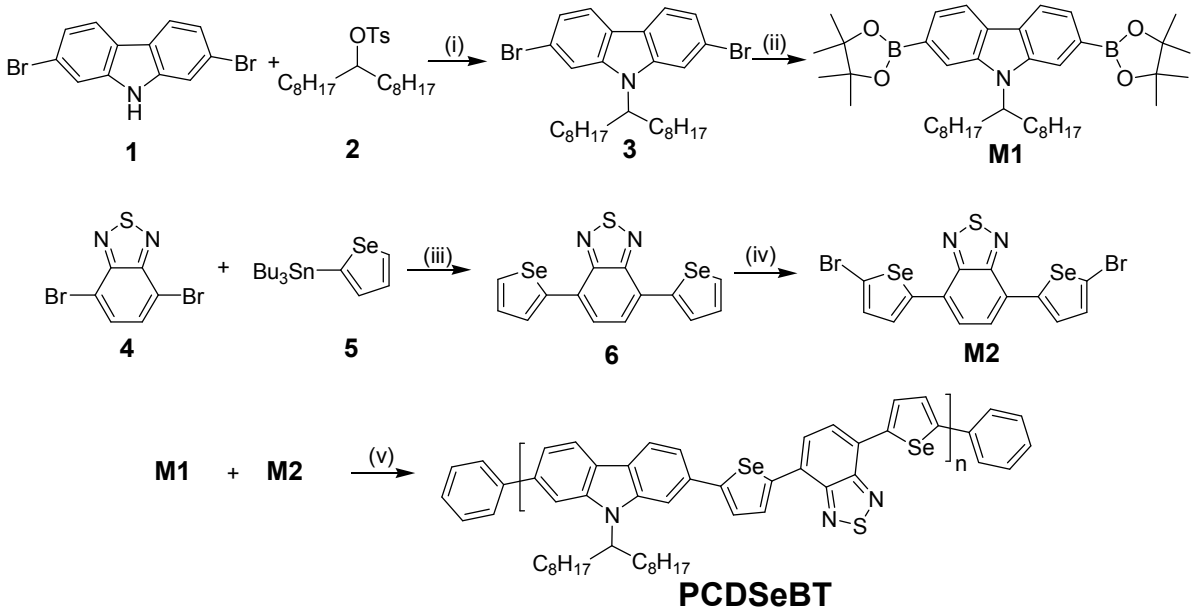

[a]Reagents and conditions: all reactions used anhydrous solvent and Ar conditions; (i) KOH, DMSO, room temperature, 6 h; (ii) 2.05 equiv. of *n*-BuLi, 2-isopropoxy-4,4,5,5-tetramethyl-1,3,2-dioxaborolane, THF, −78 °C; (iii) $Pd(PPh_3)_4$, toluene/DMF (4:1), 100 °C; (iv) NBS, DMF, room temperature, overnight; (v) $Pd_2(dba)_3$, P(*o*-Tol)$_3$, K_3PO_4, toluene/deionized H_2O (4:1), 90 °C, 3 days.

2.2.2 Optical and Electrical Properties

As shown in Figure 5a, the UV−Vis absorption spectra of **PCDSeBT** both in chloroform solution and solid state exhibit two distinct absorption bands, as typically observed for donor (D)-acceptor (A) low band gap materials. The absorption maxima (λ_{max}) of the film are located at 403 and 589 nm. The shorter absorption band is due to π−π* transitions of the polymer backbone,[30] while the lower-energy peak is attributed to intramolecular charge transfer (ICT) in the electron-rich and electron-deficient units.[31] It is worth noting that the maxima absorption values of **PCDSeBT** in the film are slightly broadened without any obvious red-shift when compared to the solution. This verifies that only a small reorganization via π−π stacking between the polymer chains is within view during the film formation because of the interchain aggregates in solution.[32] This observation is in contrast to many conjugated polymers, in which there is a red-shift that occurs in going from the solution to the solid state due to the aggregation of the polymer chains in the solid state,[22, 33] even the PCDTBT film is red-shifted by 30 nm vs. solution.[24a] Besides, the deep blue color of **PCDSeBT** solution is observed unlike the red color of PCDTBT in solution (see the digital photograph in Figure 5a). Notably, although the absorption profile of **PCDSeBT** is similar to that of the thiophene analogue, PCDTBT, the absorption onset of **PCDSeBT** is significantly red-shifted by ~70 nm, corresponding to a lower optical band gap (E_g^{opt} = 1.70 eV) than PCDTBT (E_g^{opt} = 1.85 eV). This apparently demonstrates that, in agreement with earlier studies and experimental studies,[34] the replacement of thiophene with selenophene results in a reduction of the optical bandgap due to the increase of quinoid character in the polymer backbone.[35] In a closer look of the film absorptions, it is also found that the full width at half-maximum (fwhm) of **PCDSeBT** (155 nm) is wider than that of PDCTBT (140 nm), as a matter of a characteristic of strong intermolecular Se···Se interactions, which can potentially further increase J_{SC} value. The electrochemical properties of **PCDSeBT** were investigated by cyclic voltammetry (CV). As shown in Figure 5b, **PCDSeBT** exhibits clear reversible *n*-doping/dedoping processes in the negative potential range, whereas quasi-reversible *p*-doping/dedoping behaviors in the positive potential range are observed. The HOMO and LUMO energy levels are estimated to be −5.40 eV and −3.70 eV, respectively, using the ferrocene-ferrocenium (Fc/Fc^+) redox couple (4.8 eV below the vacuum level). Both PCDTBT and **PCDSeBT** have nearly identical HOMO energy levels, but **PCDSeBT** exhibits 0.10 eV lower-lying LUMO level relative to PCDTBT (LUMO = −3.60 eV, Figure 6),[24a] verifying our presumption aforementioned about the effect of selenium on the selective fine-tuning of LUMO level. The material-design rules described by Scharber et al.[36] suggested that the PCEs of a BHJ solar cell should be much more sensitive to changes of the donor LUMO level compared to variations of the donor band gap. On the basis of the rules, the estimated PCE from the E_g^{opt} and the LUMO value of **PCDSeBT** is 7.8%. This theoretical value is much higher than that of PCDTBT (6.5%), indicating that a highly promising material for PSCs considering the frontier orbital

energies. Upon utilizing a model dimeric system containing methyl groups, the optimized molecular geometry of **PCDSeBT** and its frontier molecular orbitals of the calculated HOMO and LUMO isosurfaces were computed by density functional theory (DFT, B3LYP/6-31G) (Figure 5d). The HOMO of **PCDSeBT** is well-distributed along the conjugated chains; its LUMO is mainly centralized on BT accepting core as shaped by orbital lobes, being predicted a p-type organic semiconductor.

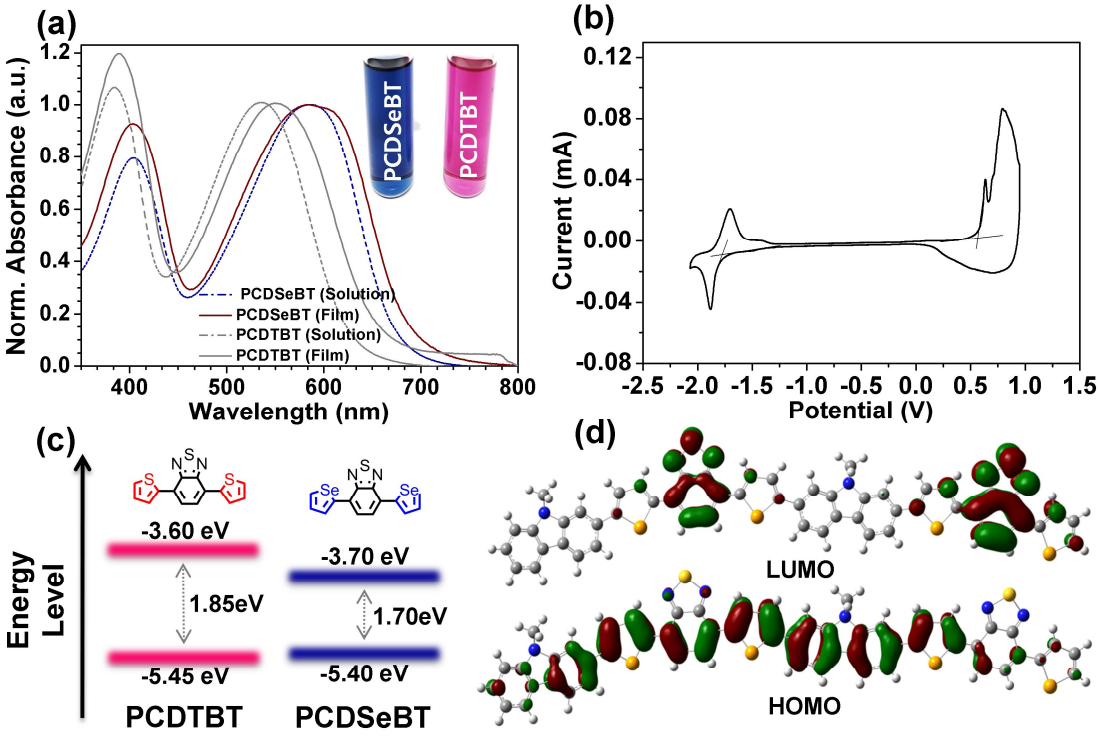

Figure 5. UV−Vis absorption spectra of **PCDSeBT** in chloroform and the thin film on the quartz (a). Inset: images of **PCDSeBT** and PCDTBT in chloroform solutions. Cyclic voltammogram of **PCDSeBT** thin film (b). Energy-level diagrams of **PCDSeBT** and PCDTBT (c). Graphical representation of a methyl-substituted **CDSeBT** dimer (d).

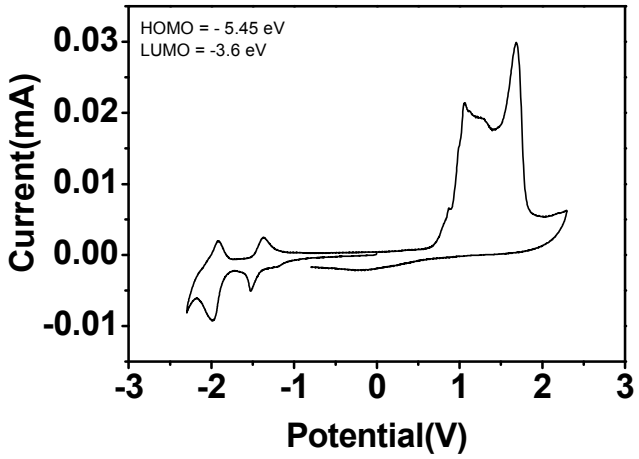

Figure 6. Cyclic voltammogram of PCDTBT thin film. Experimental conditions: values for $(E_{pa} + E_{pc})/2$ in V versus Fc/Fc^{+}; *n*-Bu_4NPF_6 (0.1 M) as supporting electrolyte; Pt wire as counter electrode; 50 mV/s scan rate.

2.2.3 Charge Transporting Properties

In order to corroborate the effect of the heteroatom substitution on charge transporting properties of the polymers, top-contact organic field-effect transistors (OFETs) were fabricated using solution processed PCDTBT and **PCDSeBT**, respectively, as the semiconducting layer on the octadecyltrichlorosilane (OTS) self-assembled monolayer (SAM)-modified Si/SiO_2 substrates (see the detailed devices fabrication in the Experimental Section). The OFET mobilities are calculated in the saturation regime using the following equation: $I_{ds} = (W/2L) \times \mu \times C_i (V_{gs} - V_{th})^2$, where W and L are the channel width and length, respectively, C_i is the capacitance per unit area of the insulation layer. Linear plot of $I_{ds}^{1/2}$ vs. V_{gs} deduced from the I_{ds} vs. V_{gs} measurement. These devices show characteristics of a typical *p*-channel transistor with good drain-current Modulation, well-defined linear, and saturation regions (Figure 7). The summary of the performances is provided in Table 1. The OFET device using as-cast PCDTBT films without thermal annealing exhibits a hole mobility of 2.2×10^{-4} $cm^2/V \cdot s$ with an on/off current ratio (I_{on}/I_{off}) of 4.44×10^3. For PCDTBT thin films after annealing at evaluated temperatures, the mobilities are not markedly improved, implying that the PCDTBT thin films remain nearly amorphous for both as-cast and annealing at high temperature. On the other hand, it is found that the unannealed thin films of **PCDSeBT** exhibit a slightly higher mobility of $\mu_h = 5.1 \times 10^{-4}$ $cm^2/V \cdot s$, compared with that of pristine PCDTBT. Interestingly, in contrast, as the **PCDSeBT** thin films are annealed at a temperature of 120 and 150 °C, the mobilities are systematically improved up to 1.0×10^{-3} $cm^2/V \cdot s$ (Figure 7b), which is about 1 order of magnitude higher than that of PCDTBT, possibly due to increased interpolymer chain contact induced by Se···Se interactions with the thermal annealing process.

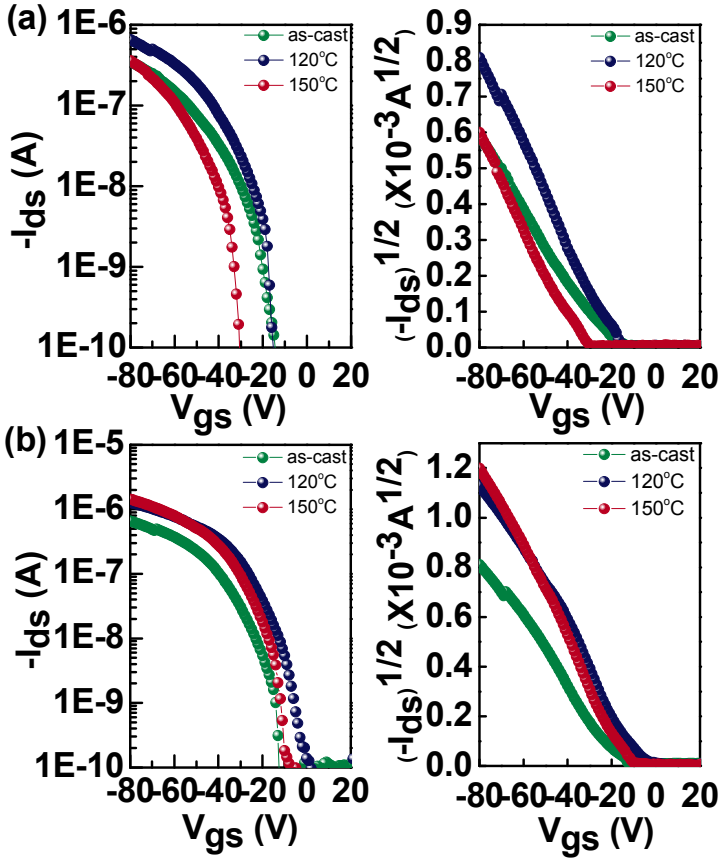

Figure 7. Transfer characteristics of (a) PCDTBT- and (b) **PCDSeBT**-based OFET devices at different annealing temperatures.

Table 1. OFET performance of PCDTBT and PCDSeBT polymer thin films at different annealing temperatures.[a]

polymer	condition	mobility (μ_h) (cm2/V·s)	I_{on}/I_{off}[b]	V_{th} [V]
PCDTBT	as-cast	2.2×10^{-4}	2.2×10^{3}	-21
	120 ºC	4.9×10^{-4}	7.9×10^{3}	-22
	150ºC	3.5×10^{-4}	7.9×10^{3}	-34
PCDSeBT	as-cast	5.1×10^{-4}	4.1×10^{4}	-19
	150ºC	7.8×10^{-4}	3.4×10^{4}	-9
	120ºC	1.0×10^{-3}	4.0×10^{4}	-13

[a]All device characteristics were obtained from the devices (L = 50 μm and W = 1.5 mm) based on OTS-treated Si/SiO_2 substrates. [b]The on/off current ratio (I_{on}/I_{off}) were extracted from the linear-regime transfer characteristics.

2.2.4 Crystallinity

To gain a better understanding of the influence of the thermal annealing, the crystallinity and molecular organization of PCDTBT and **PCDSeBT** thin films were investigated by X-ray diffraction (XRD), both before and after annealing at 150 °C. Both the as-cast and annealed PCDTBT thin films fail to reveal any defined scattering patterns (Figure 8a), indicating the macroscopically disordered, amorphous structure. In the case of **PCDSeBT**, the as-cast thin films show very weak diffractions (Figure 8b). Upon thermal annealing, the primary peak at 4.42°, corresponding to a *d*-spacing of 19.99 Å, progressively intensifies and the secondary broad peak at ~21.1° (d = 4.21 Å) that is probably related to π–π stacking becomes visible (Figure 8b). On the basis of these XRD results, we can conclude that the oriented microstructure of the as-cast **PCDSeBT** thin films is kinetically limited but the polymer chains reorganize to ordered lamellar packing structures upon annealing. This observation is a plausible explanation for the sudden rise in mobility of **PCDSeBT** as a function of the thermal annealing.

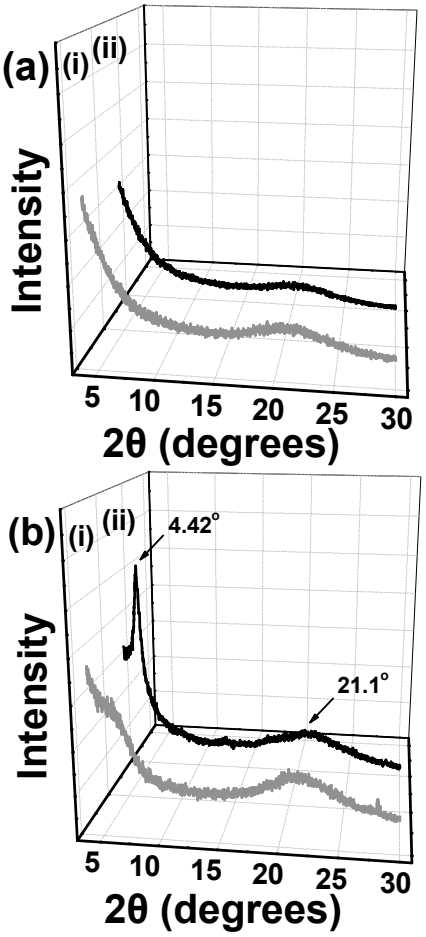

Figure 8. X-ray diffraction patterns of PCDTBT (a) and **PCDSeBT** (b) thin films before (i) and after annealing at 150 °C (ii), respectively.

2.2.5 Photovoltaic Effects

Photovoltaic effects of **PCDSeBT** were investigated in BHJ PSCs with the device structures of the standard configuration glass/ITO/PEDOT:PSS/**PCDSeBT**:$PC_{71}BM$/Al. The **PCDSeBT**:$PC_{71}BM$ weight ratio was optimized from 1:1, 1:2, 1:3, to 1:4. The current-density-voltage (*J-V*) characteristics of the devices under the illumination of simulated AM 1.5G conditions (100 mW/cm^2) are shown in Figure 9a and the parameters are summarized in Table 2. Without extensive optimization, the initial device fabricated from the blend solutions with a **PCDSeBT**:$PC_{71}BM$ weight ratio of 1:1 shows a PCE of 0.73% with a J_{SC} of 2.98 mA/cm^2, a V_{OC} of 0.71 V, a fill factor (*FF*) of 35%. As increasing the weight fraction of $PC_{71}BM$, the PCEs are gradually increased. The device containing the 1:4 w/w blend as the photoactive layer after thermal annealing at 150 °C delivers at superior performance with the J_{SC} of 11.7 mA/cm^2, V_{OC} of 0.79 V, and FF of 45%, improving the PCE to 4.12%, an approximately 37% enhance enhancement in PCE, when compared to the reference cell based on PCDTBT:$PC_{71}BM$ for the sake of comparison (Figure 10). It is worth noting that the J_{SC}, to the best of our knowledge, is among the highest J_{SC}s reported to date for PCSs based on PCDTBT analogues,[24, 26, 37] in a good agreement with the extended absorption of sunlight through the low band gap and broaden absorption band of **PCDSeBT**. In order to ensure the accuracy of the measurements, we investigated the incident photon-to-current efficiency (IPCE) spectrum of the optimized device (1:4 w/w), exhibiting over 65% at the energetically lower peak, i.e. at the λ_{max} of **PCDSeBT** (Figure 9b). The J_{SC} value calculated by integrating the IPCE data with an AM 1.5G reference spectrum is rather consistent with that obtained from *J-V* plots within 10% error.

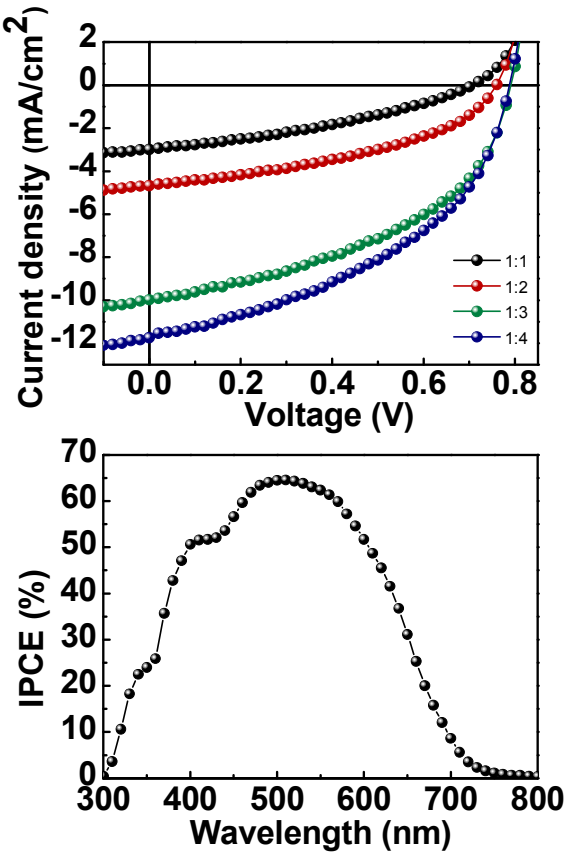

Figure 9. *J*−*V* characteristics of PSCs based on **PCDSeBT**:$PC_{71}BM$ under illumination of AM 1.5G, 100 mW/cm^2 (a). Incident photon to current efficiency (IPCE) spectrum of **PCDSeBT**:$PC_{71}BM$ (1:4 w/w)-based device (b).

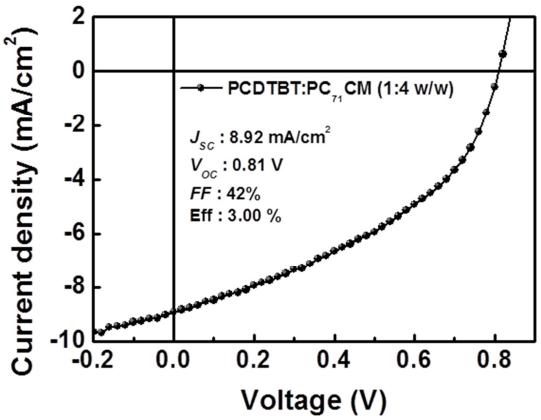

Figure 10. *J-V* characteristics of PSC based on PCDTBT:$PC_{71}BM$ under illumination of AM 1.5 G, 100 mW/cm^2 .

Table 2. Photovoltaic Properties of PSCs Based on PCDSeBT.

PCDSeBT:$PC_{71}BM$	J_{sc} (mA/cm^2)	V_{oc}	*FF*	PCE (%)
(1:1)	2.98	0.71	0.35	0.73
(1:2)	4.66	0.76	0.42	1.50
(1:3)	9.97	0.79	0.46	3.64
(1:4)	11.7	0.79	0.45	4.12
(1:4)[a]	10.3	0.64	0.42	2.76

2.2.6 Atomic Force Microscopy

Atomic force microscopy (AFM) was performed to gain insight into the surface morphology of the optimized 1:4 w/w blend films (Figure 11). The films before and after thermal annealing have smooth surface topographies and very similar features, where the formation of voids, typically attributed to incompatibility between donor and acceptor components, is not observed. However, the rms roughness is somewhat reduced to from 0.47 to 0.43 nm with thermal treatment, being favorable for charge separation and transport. This can reasonably explain the enhanced efficiency via the post-annealing effect. Note that, in stark contrast to PCDTBT:$PC_{71}BM$ system in which thermal annealing reduced the photovoltaic parameters (*FF*, J_{SC}, and V_{OC}),[24b, 38] the performance of all **PCDSeBT**-based devices for this study is considerably improved as a result of thermal treatment. We can conclude that the formation of crystalline nanoscale domains would be slightly induced in **PCDSeBT**:$PC_{71}BM$ with a thermal treatment in consequence of the ordered crystalline nature of the **PCDSeBT** on annealing as supported by the XRD results above as well as the large quinoidal character in the polymer backbone as the inclusion of selenophene.[39] The AFM of the annealed film gives an evidence for slightly nanofibril-like organization (see Figure 11b).

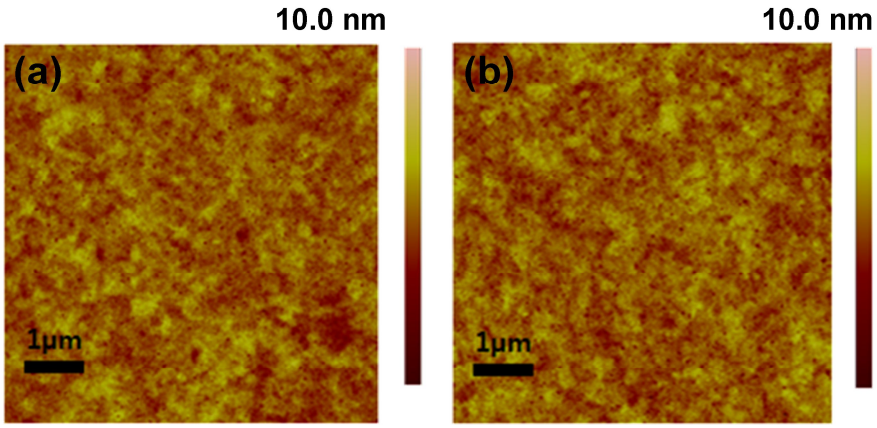

Figure 11. AFM images (6 μm × 6 μm) of **PCDSeBT**:$PC_{71}BM$ (1:4 w/w) cells before (a) and after (b) thermal annealing at 150 °C.

2.2.7 Hole and Electron Mobilities

The hole and electron mobilities of **PCDSeBT**:$PC_{71}BM$ (1:4 w/w) blends were measured using the space-charge-limited current (SCLC) method and the *J*−*V* characteristics were plotted in Figure 12. The hole mobility (μ_{hole} = 4.68 × 10^{-5} cm^2/V·s) obtained with the thermally annealed film is one order higher than that without post annealing (μ_{hole} = 4.02 × 10^{-6} cm^2/V·s), whereas in the both cases, the electron mobilities ($\mu_{electron}$) are similar (1.24 × 10^{-3} and 5.58 × 10^{-3} cm^2/V·s) for as-cast and annealed films, respectively, yielding a smaller difference between the mobility ratio for the annealed film. The higher mobilities and more balanced charge transport should definitely favor the charge transportation in the blend film and lead to high solar cell performance, supporting the beneficial effect of the thermal annealing on **PCDSeBT**:$PC_{71}BM$ cells.

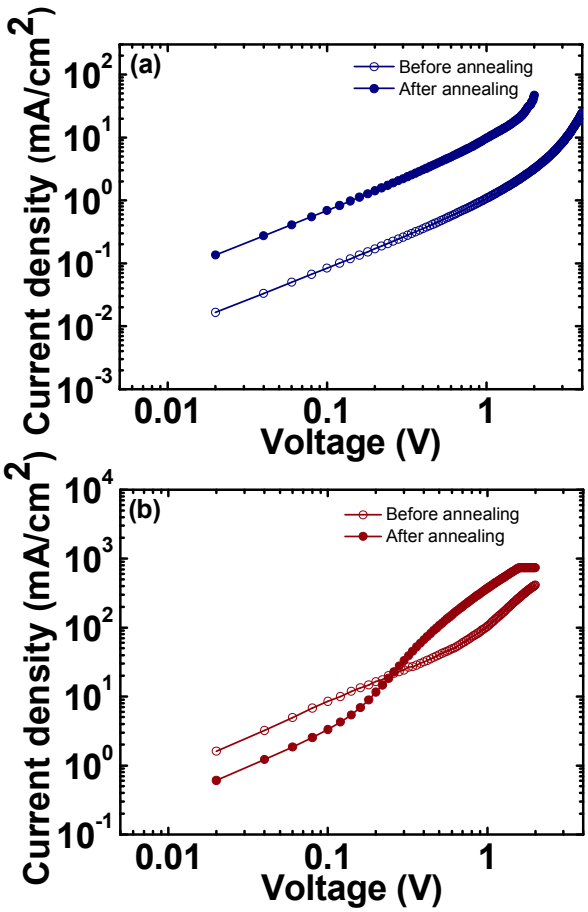

Figure 12. *J-V* characteristics measured by the space charge limited current (SCLC) method with **PCDSeBT**:$PC_{71}BM$ (1:4 w/w) films under dark conditions before and after thermal annealing for hole-only device (a) and electron-only device (b).

2.3 Conclusion

In conclusion, diselenienylbenzothiadiazole (DSeBT) units have successfully been incorporated into a D−A polymer backbone by Suzuki polymerization with 2,7-carbazole comonomer, affording a poly(2,7-carbazole-alt-diselenienylbenzothiadiazole) (**PCDSeBT**); This design motif is that replacement of thiophenes to selenophene units in PCDTBT that acts as a superior *p*-type photoactive material for PSCs, induces a lower band gap (1.70 eV) than that of PCDTBT (1.85 eV), while the ideal HOMO energy level (−5.40 eV) is still maintained. Another pleasant surprise comes from **PCDSeBT** with a relative wider absorption band observed, as a result of strong intermolecular Se···Se interactions. The lower band gap with the broaden absorption band significantly improves a J_{SC} of 11.7 mA/cm^2, which is among the highest J_{SC} values for PSCs based on PCDTBT derivatives, while the low HOMO energy level maintains the high V_{OC} value. The corresponding PCE is 4.12%, about 37% higher than that obtained from a PCDTBT-based reference device. This work provides a feasible strategy for selective fine-tuning of LUMO levels, which achieves a high J_{SC} value, while nearly remaining a high V_{OC}. Therefore, further exploration of **PCDSeBT**-based PSCs is still warranted for high-performance PCEs by means of controlling the film morphology and improving electric contacts.

Chapter Ⅲ. Heteroarene Dodecyldithieno[2,3-*b*;7,6-*b*]carbazole-Based Polymers

3.1 Introduction

Many more high-performance polymers have been developed in recent years. The research about not only to reduce the band gap of donor materials but also to increase hole mobility is on the progress. Especially, fused aromatic molecules are in the spotlight as donor materials with high mobility. Some fused aromatic molecules, such as pentacene and S containing heteroarenes,[30, 40] display mobility over 1 $cm^2/(V\cdot s)$ due to their strong intermolecular π-π interaction in the crystalline state. It is believed that integrating these units into conjugated polymers might render the materials high mobility.[41] Notably, several thiophene-based conjugated polymers comprising S-containing heteroarenes have been reported, because S-containing fused aromatics has better stability than benzene-based acene as well as can prevent twisting between the adjacent aromatic units in the polymer backboned. However, with the increase of the size of the S-containing heteroarenes, density of the alkyl chains along the polymer chain decreases, which may result in the low solubility of the polymers.

In order to solve this problem, carbazole which is one of important aromatic units for designing high-performance polymers solar cells[42] were introduced, since the nitrogen atom in the carbazole can allow introducing more alkyl chains into the polymer chins for improving solubility.

Here, eight alternating conjugate polymers comprising a S- and N-containing heteroarene, i.e, *N*-9′ heptadecanyldithieno[2,3-*b*;7,6-*b*]carbazole and a series of conjugated polymers as donor polymers with higher hole mobility (**PTCZTBT**, **PTCZTfBT**, **PTCZTffBT, PTCZTTT**, **PTCZTPT**, **PTCZTQ**, **PTCZTfQ, PTCZTffQ)** were synthesized by Stille coupling reaction with $Pd_2(dba)_3$/P(*o*-tol)$_3$ as catalyst in the yield of 57.8−91.8%. The crude polymers were purified by reprecipitation and Soxhlet extraction, after purification, gel-permeation chromatography (GPC) analysis exhibits number-averaged molecular mass (M_n) of 11000−67000 g/mol with polydispersity (PDI) of 1.25−2.83. All polymers were readily soluble in common solvents such as chloroform, toluene, THF, and chlorobenzene.

3.2 Results & Discussion

3.2.1 Synthesis

The synthesis of *N*-9′-Heptadecanyldithieno[2,3-*b*;7,6-*b*]carbazole and polymers is outlined in scheme 4. Compounds **8** was synthesized according to the previously reported procedure.[24a] *N*-9′-Heptadecanyl-2,7-dibromo-3,6-diiodocarbazole (**9**) was prepared by the iodination of compound **8** with KI/KIO_3 in acetic acid in a yield of 84.05%, which reacted with trimetylsilylacetylene in a typical Sonogashira reaction condition to give *N*-9′-Heptadecanyl-2,7-dibromo-3,6-di(trimetylsilyethyny)carbazole (**10**) in a yield of 60.2%. The cyclization reaction in the presence of Na_2S in NMP at 190 °C obtained *N*-9′-Heptadecanyldithieno[2,3-*b*;7,6-*b*]carbazole (**11**) in a yield of 68.9%. The key building block *N*-9′-Heptadecanyl-3,8-bis(trimethylstannyl)dithieno[2,3-*b*;7,6-*b*]carbazole (**TCZT**) was synthesized by deprotonation with *n*-BuLi at −78 °C followed by quenching with trimethyltin chloride. The target polymers (**PTCZTBT**, **PTCZTfBT**, **PTCZTffBT, PTCZTTT**, **PTCZTPT**, **PTCZTQ**, **PTCZTfQ, PTCZTffQ**) were synthesized by Stille coupling reaction between TCZT and benzothiadiazole/thienothiophene/thienopyrroldione/quinoxaline derivatives with $Pd_2(dba)_3$/P(*o*-tol)$_3$ as catalyst at 120 °C for 48 h in the yield of 57.8−91.8%. The crude polymers were purified by reprecipitation and Soxhlet extraction with methanol, acetone, hexane, and chloroform. Details of synthesis of monomers, polymerization, and their characterizations are given in the Experimental Section. After purification, gel-permeation chromatography (GPC) analysis against PS standard exhibits number-averaged molecular mass (M_n) of 11000−67000 g/mol with polydispersity (PDI) of 1.25−2.83. All polymers were readily soluble in common solvents such as chloroform, toluene, THF, and chlorobenzene.

Scheme 4. Synthetic route to **TCZT** and **its polymers**[a].

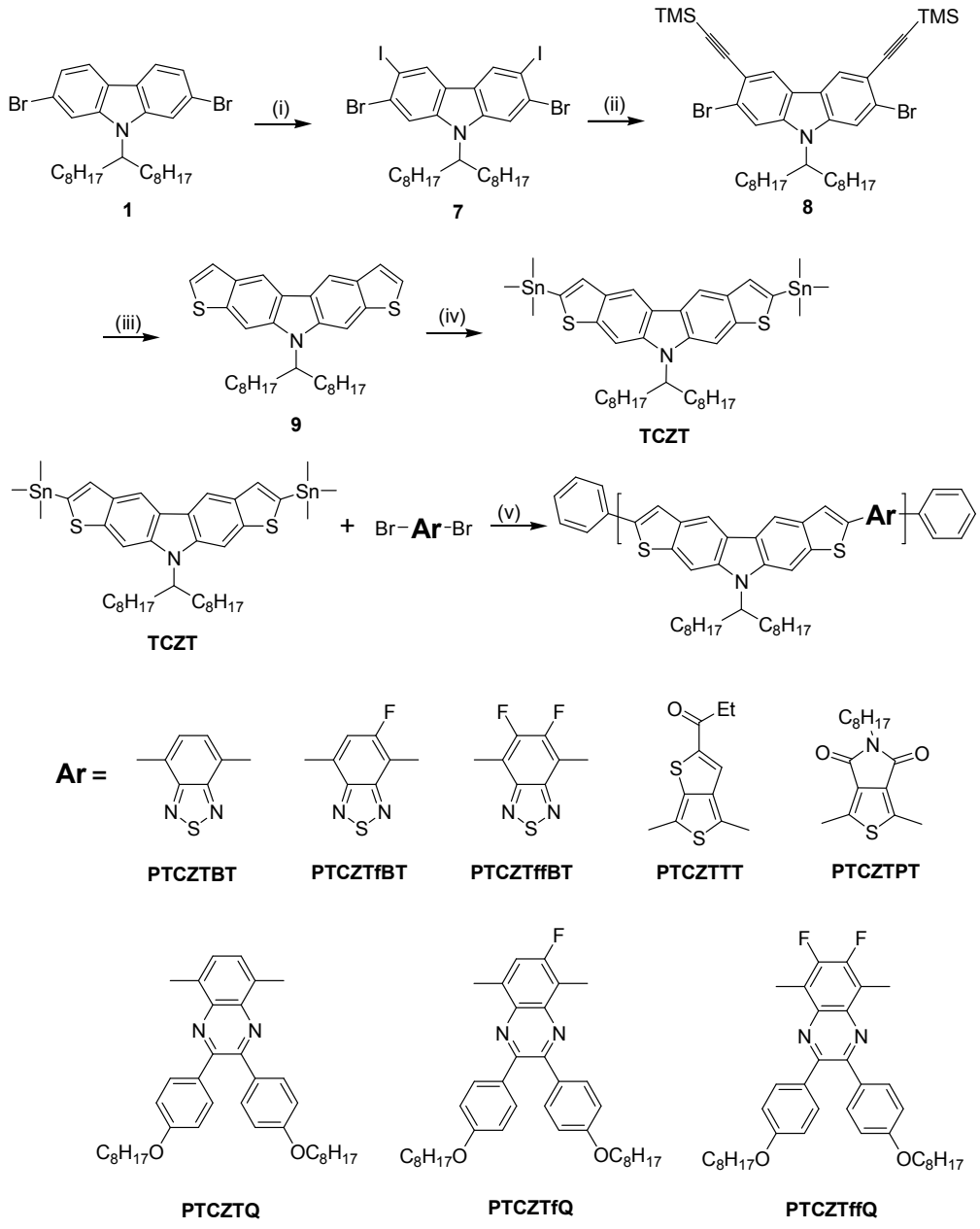

[a]Reagents and conditions: all reactions used anhydrous solvent and Ar conditions; (i) KI, KIO_3, AcOH, 80 °C, 6h; (ii) $Pd(PPh_3)_2Cl_2$, CuI, Et_3N, THF, trimetylsilylacetylene, room temperature, 48 h; (iii) $Na_2S{\cdot}9H_2O$, NMP, 190 °C, 12 h; (iv) 2.5 equiv. of *n*-BuLi, trimethyltin chloride, THF, −78 °C; (v) $Pd_2(dba)_3$, P(*o*-Tol)$_3$, K_3PO_4, toluene, 120 °C for 48 h.

3.2.2 Optical Properties

The photophysical properties of TCZT's polymers were investigated both in chloroform solution and in thin films, which are shown in Figure 13. Benzothiadiazole derivative polymers (**PTCZTBT**, **PTCZTfBT**, **PTCZTffBT**) and quinoxaline derivative polymers (**PTCZTQ**, **PTCZTfQ**, **PTCZTffQ**) showed two absorption peaks, which is a common feature of D-A copolymers. The absorption peaks at short wavelength (360 nm) originate from π-π* transition of their conjugated backbone, while the absorption peaks at long wavelength (556−596 nm) could be attributed to the strong intramolecular charge transfer (ICT) interaction between the dithieno[2,3-*b*;7,6-*b*]carbazole donors and benzthiadiazole/quinoxaline derivative acceptors. The ICT absorption peaks of **PTCZTBT**, **PTCZTfBT**, **PTCZTffBT**, **PTCZTQ**, **PTCZTfQ**, and **PTCZTffQ** appeared at 574 nm, 596 nm, 560 nm, 563nm, 558 nm, and 558 nm, respectively. Especially quinoxaline derivative polymer's observed at almost same range while the peak intensity of ICT absorption was gradually increased in order of **PTCZTQ**, **PTCZTfQ**, **PTCZTffQ.** It means that the more substitution of fluorine atoms to the quinoxaline moiety makes possible the more light absorption. In case of benzothiadiazole derivative polymers, **PTCZTfBT** containing one fluorine atom showed a red-shift than **PTCZTBT** and at the same time intensity is also increased. However, **PTCZTffBT** containing one fluorine atom showed a blue-shift. **PTCZTTT** also showed two absorption peaks but its ICT peak showed very low intensity at 565 nm in contrast with benzothiadiazole derivative polymers and quinoxaline derivative polymers. **PTCZTPT** showed only one peak at 503 nm. The film absorption of the polymers except for **PTCZTffQ** which had extremely broad absorption peak range showed the same absorption peak with its solution state. This verifies that only a small reorganization via π−π stacking between the polymer chains is within view during the film formation because of the inter-chain aggregates in solution.[32]

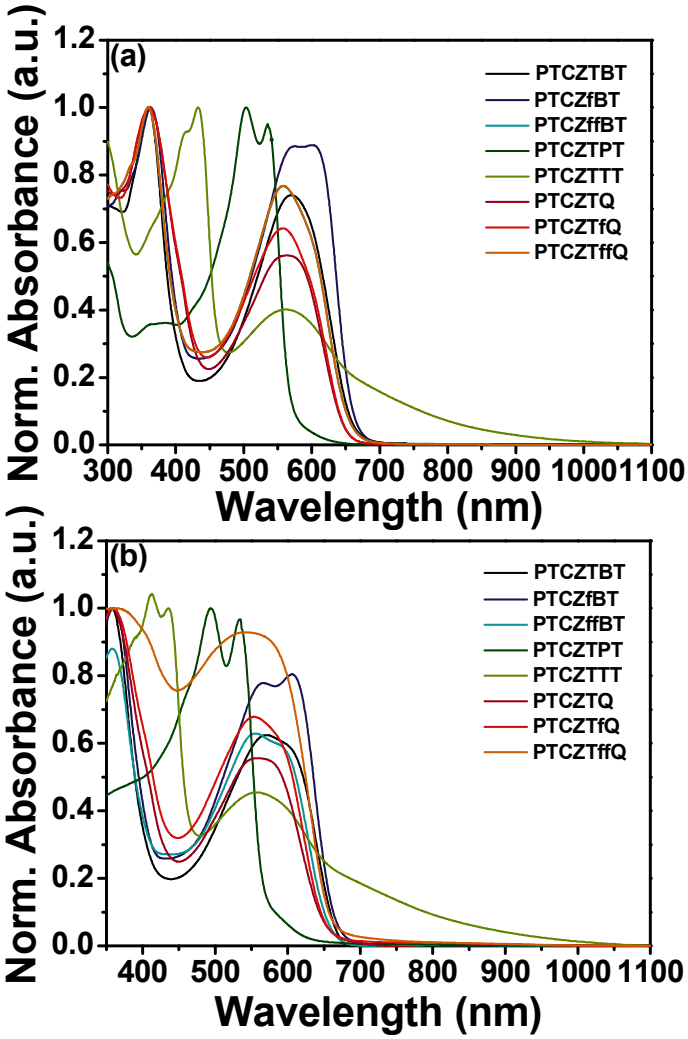

Figure 13. UV-Vis absorption spectra of **TCZT's polymers** in $CHCl_3$ (a) and the thin film on the quartz (b).

3.3 Conclusion

TCZT's polymers (**PTCZTBT**, **PTCZTfBT**, **PTCZTffBT, PTCZTTT**, **PTCZTPT**, **PTCZTQ**, **PTCZTfQ, PTCZTffQ)** comprising a S- and N-containing heteroarene, i.e, *N*-9′-heptadecanyldithieno[2,3-*b*;7,6-*b*]carbazole expected to have high hole mobility were gained by Stille coupling reaction between TCZT and benzothiadiazole/thienothiophene/thienopyrroldione/ quinoxaline derivatives with $Pd_2(dba)_3/P(o\text{-tol})_3$ as catalyst in the yield of 57.8−91.8%. The crude polymers were purified by reprecipitation and Soxhlet extraction, after purification, gel-permeation chromatography (GPC) analysis exhibits number-averaged molecular mass (M_n) of 11000−67000 g/mol with polydispersity (PDI) of 1.25−2.83. All polymers were readily soluble in common solvents such as chloroform, toluene, THF, and chlorobenzene.

Chapter Ⅳ. Synthesis and characterization of a bis-methanofullerene-4-nitro-α-cyanostilbene dyad as a potential acceptor for high-performance polymer solar cells

In this chapter, we report the synthesis, characterization, and electrochemical properties of **bis-PCBM dyad** containing 4-nitro-α-cyanostilbene units for potential usage in efficient organic solar cells. The bis-PCBM dyad is fully characterized by NMR, UV−Vis absorption, and electrochemical cyclic voltammetry. It is found that the presence of 4-nitro-α-cyanostilbenes affects the cyclic voltammetry and absorption spectrum very little. Whereas the 56 π-electron system in the bis-functionalized fullerene cage significantly influences on the electrochemical and photophysical properties, resulting in up-shifted LUMO and wider absorption compared to PCBM. Although the efficiencies of both conventional and the inverted cells based on P3HT/**bis-PCBM dyad** as the preliminary results are low in comparison with the optimized high-performance PSCs, it is believed that the efficiency would be improved through successful device optimization of P3HT/**bis-PCBM dyad** cells.

4.1 Introduction

A soluble C_{60} derivative, [6,6]-phenyl-C_{61} butyric acidmethyl ester (PCBM) has affirmed to be an invaluable *n*-type semiconductor for solution-processed organic electronics.[15, 43] Therefore, PCBM has represented the well-studied benchmark acceptor in bulk hetero-junction (BHJ) polymer solar cells (PSCs).[17, 21, 44] Although the modification of the PCBM's structure by changing the substituents aiming at more efficient acceptor materials for PSCs has come into focus, most of the device performance is poorer than or similar to that of PCBM.[17c, 19a, 19c, 45] An important breakthrough was achieved when PCBM was replaced by bis-functionalized 56 π-electron fullerenes[46], such as bis-PCBM16 and bis-indene-C_{60} adducts.[46a, 46e] These bis-adducts possess higher LUMO energy levels, resulting in higher V_{OC} as well as higher power conversion efficiency (PCE) of the P3HT-based PSCs.[46a, 46d, e] Another important development was accomplished by the synthesis of [6,6]-phenyl-C_{71} butyric acid methyl ester ($PC_{71}BM$) that has a broader absorption in the visible region than PCBM, leading to a positive effect on current generation in PSCs.[17a, 47] Despite the enormous advances in the synthesis of fullerene based dyads and triads to further increase visible absorption,[48] limited success in PSCs has been reported since most of the light harvesting organofullerenes suffer from negative side effects, such as insufficient charge transport, inefficient charge dissociation, or morphology problems.[45b, 46d] To date, only fullerene-4-nitro-α-cyanostilbene dyad showed superior photovoltaic performance to that of the traditional PCBM.[49] In this context, we have designed and synthesized a **bis-PCBM dyad** incorporating 4-nitro-α-cyanostilbene units. Considering possible combined effects from the π-electron system by the bis-adduct framework and the increased light absorption in the visible region by the additional chromophores, the **bis-PCBM dyad** is rationally expected to display excellent performance and its structural motif is outlined in Figure 14.

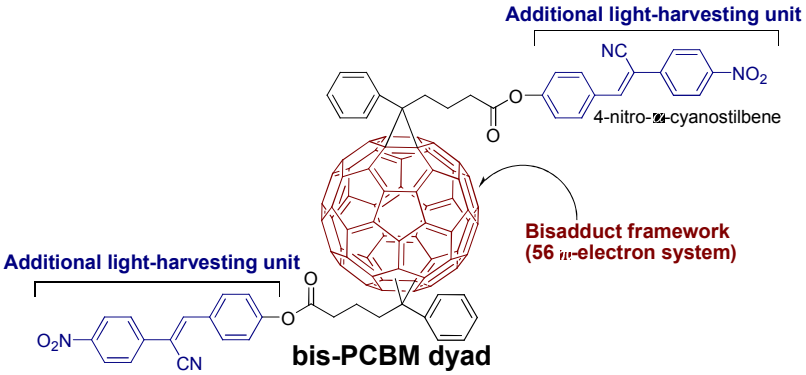

Figure 14. Rational design motif of **bis-PCBM dyad**; 4-Nitro-α-cyanostilbene was chosen as additional light-harvesting unit to provide a higher J_{sc}. In principle, the LUMO can be raised by bis-adduct framework due to 56 π-electron system.

4.2 Results & Discussion

4.2.1 Sythesis

The synthesis of the intermediates and **bis-PCBM dyad** is shown in Scheme 5. Previously, Sharma and co-workers prepared the 4-nitro-4-hydroxy-α-cyanostilbene as a dark green solid *via* Knoevenagel condensation between 4-hydroxybenzaldehyde and 4-nitrobenzylcyanide in ethanol in the presence of sodium hydroxide.[50] Later, aiming at improving the PSCs, they reported the synthesis and evaluation of a 4-nitro-α-cyanostilbene-based PCBM, which, given its high device performance, identified a new effective modification strategy for fullerenes in PSCs.[49]

Scheme 5. Synthetic route to **bis-PCBM dyad**.

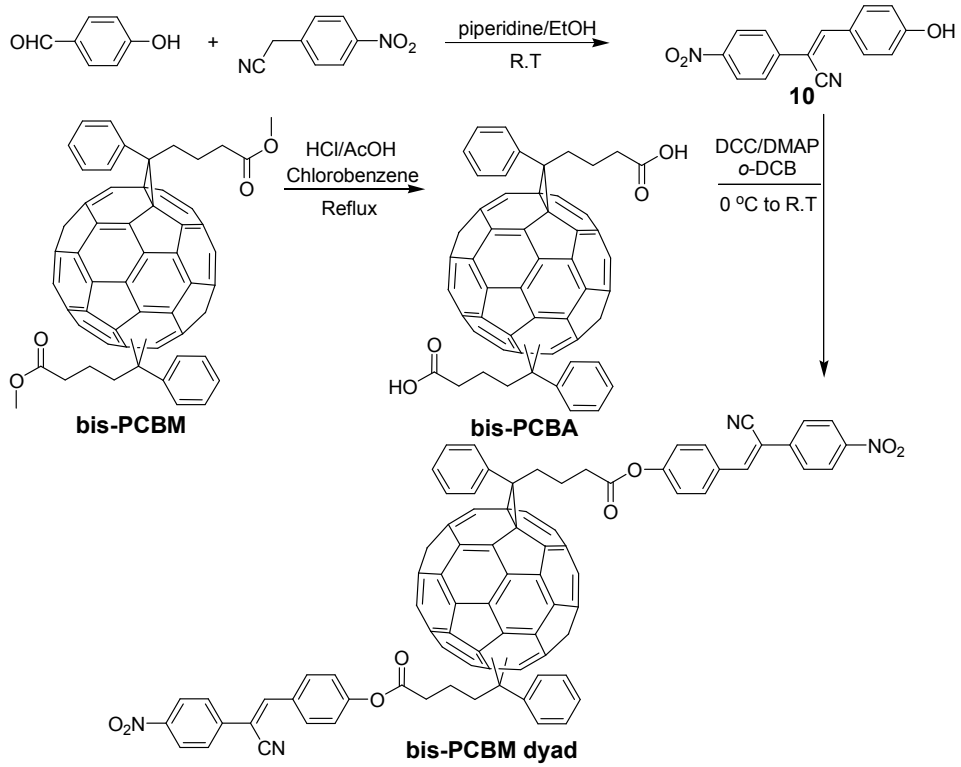

However, our initial attempt to synthesize 4-nitro-4-hydroxy-α-cyanostilbene by the procedure described in the literature above, gave, by the inspection of the ^{1}H NMR spectrum, inseparable complex mixtures. Despite the utilization of various purification tools, the pure greenish product could not be isolated. A characteristic solubility of the mixtures in water was a main problem of the product separation. This is probably due to the formation of salt sodium phenoxides since sodium hydroxide is strong enough base to react with 4-hydroxybenzaldehyde as acidic phenolic compound. We then proceeded to investigate the synthesis of 4-nitro-4-hydroxy-α-cyanostilbene (**10**) through the

Knoevenagel reaction catalyzed by piperidine in ethanol, successfully affording a pure 'red' product in quantitative yield, an observation at odds with the color reported by Sharma et al. (see the digital photograph and ^{1}H NMR in Figure 15a). As well, bis-PCBM was obtained as a by-product of the preparation of PCBM.[43a, 46d] After isolating the unreacted C_{60} and PCBM by column chromatography in the regular manner, the isomeric bis-PCBMs were collected upon elution with dichloromethane. And then, the esters were hydrolyzed with hydrochloric acid/acetic acid to the corresponding dicarboxylic acid-functionalized bis-PCBA. The acid bis-PCBA was found to be insoluble in most organic solvents, most likely due to the combination of intermolecular hydrogen bonding and C_{60}-C_{60} interactions.[43a] Finally, **bis-PCBM dyad** was prepared by a Steglich esterification (DCC/DMAP)[51] of **10** with bis-PCBA. The structure of **bis-PCBM dyad** was fully identified by ^{1}H and ^{13}C NMR (Fig. 1b and c). Owing to two large substituents, the target product is easily soluble in chloroform, tetrahydrofuran (THF), chlorobenzene (CB) and *ortho*-dichlorobenzene (*o*-DCB). In contrast to the color previously described for 4-nitro-α-cyanostilbene-PCBM (dark green), the obtained product **bis-PCBM dyad** turned out to be a dark red solid (see the digital photograph in Figure 3b). In the ^{1}H NMR spectrum, as a result of the successful ester formation, we can clearly see a disappearance of the δ_{OH} resonances at 5.75 ppm as well as an apparent up-field shift of the peaks (δ = 6.98 ppm) denoting the aromatic signals ortho to the phenolic benzene ring unit in 4-nitro-4-hydroxy-α-cyanostilbene. The ^{13}C NMR spectroscopy shows a resonance in the carbonyl region at δ = 170.22 ppm and a lot of carbon signals in the sp^2 region (δ = 127−150 ppm). Additionally, the spectrum displays two single intensity resonances assigned to sp^3-hybridized bridgehead carbon atoms at δ = 79.83 ppm and 79.25 ppm as well as signals at around 50 ppm corresponding to the quaternary carbon atoms of the fullerene unit, in accordance with a [6,6]-closed methanofullerene. The remaining signals are attributable to the carbon atoms of the butyl chains in PCBM.

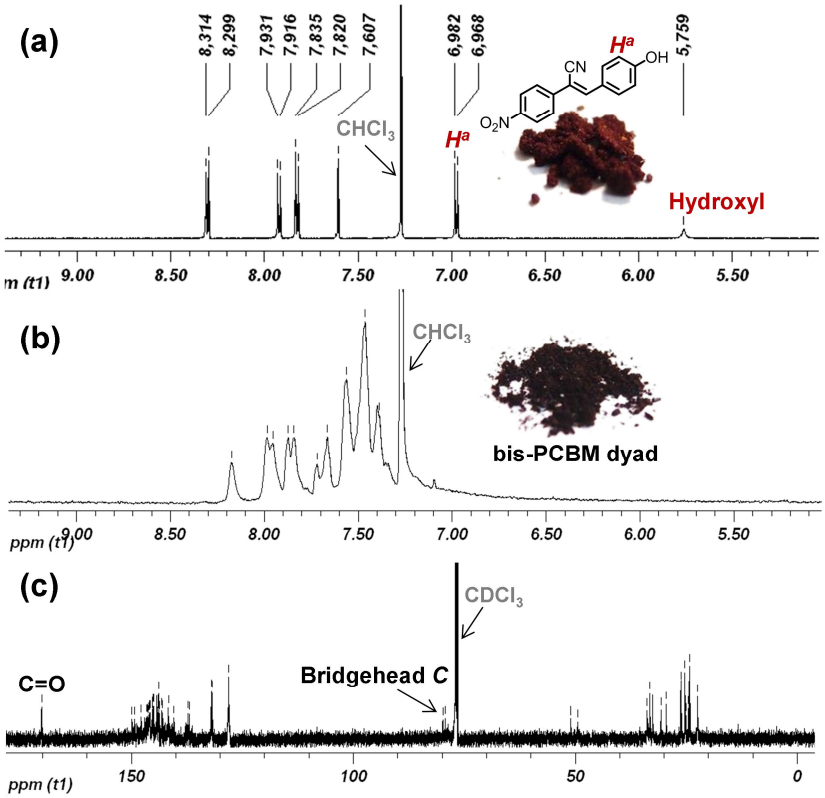

Figure 15. ^{1}H NMR (a) of **10** and ^{1}H and ^{13}C NMR (b, c) spectra of **bis-PCBM dyad** in $CDCl_3$. The digital photographs of **10** and **bis-PCBM dyad**.

3.2.2 Optical Poperties

Figure 16 depicts the UV−Vis absorption characteristics of 4-nitro-4-hydroxy-α-cyanostilbene (**1**), PCBM, bis-PCBM, and **bis-PCBM dyad** in chloroform solution. PCBM shows strong absorption at 330 nm whereas the absorption maximum of **10** is at 365 nm. The absorption of **bis-PCBM dyad** is non-superimposable on the sum of the absorption spectra of **10** and bis-PCBM (see bis-PCBM in Figure 16 as well), implying an evidence of the electronic interaction of the two chromophores.[52] Interestingly, the spectrum of **bis-PCBM dyad** displays an increased and wider absorption compared to PCBM, with a shoulder peak at ca. 430 nm as characteristic of [6,6]-closed ring isomer. The relatively higher absorption of **bis-PCBM dyad** in the visible region can be attributed, in part, to a highly broken symmetry of the fullerene core, leading to the lowest-energy transitions being formally dipole allowed.[53] A closer view of the two spectra (PCBM and **bis-PCBM dyad**) discloses, furthermore, a red-shifted band at ~707 nm relative to the PCBM (697 nm). From the herein observed spectral features, it is safe to assume that **bis-PCBM dyad** would be able to absorb more solar energy and contribute to an improved performance.

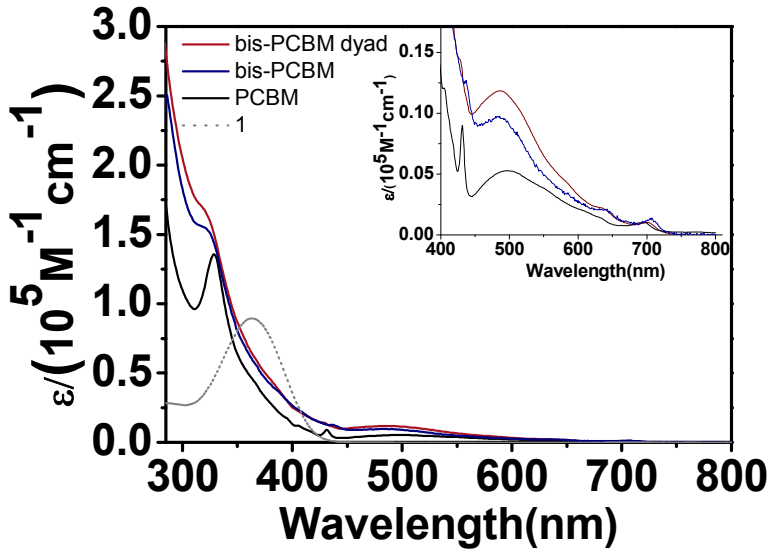

Figure 16. UV−Vis absorption of **10**, PCBM, bis-PCBM, and **bis-PCBM dyad** in $CHCl_3$ solution.

4.2.3 Electrical Properties

The electrochemical properties of **bis-PCBM dyad** were studied by cyclic voltammetry (CV), where PCBM data obtained in this study for comparison is also shown in Figure 17. In *o*-DCB, each compound exhibits three well-defined, single-electron, quasi-reversible waves, which is in sharp contrast with the results reported for 4-nitro-α-cyanostilbene-PCBM with only one reduction peak.[49] The half-cell potentials (defined as $E_1 = (E_{pc} + E_{pa})/2$) for the reduction of the PCBM and **bis-PCBM dyad** relative to Fc/Fc^+ are −1164, −1540, −2036 mV, and −1261, −1587, −2260 mV, respectively. The **bis-PCBM dyad** lifts its LUMO level by ~100 meV, from −3.636 eV (PCBM) to −3.539 eV, because of the extraction of two more π-electrons from the fullerene core. This reveals an obvious similarity to the difference between LUMO levels of PCBM and bis-PCBM.[46d] We do not observe an additional up-shift of the LUMO because of the inductive effect of the strong electron withdrawing nitro and cyano groups in the **bis-PCBM dyad** on the redox behavior, as opposed to the report by Sharma et al.[49]

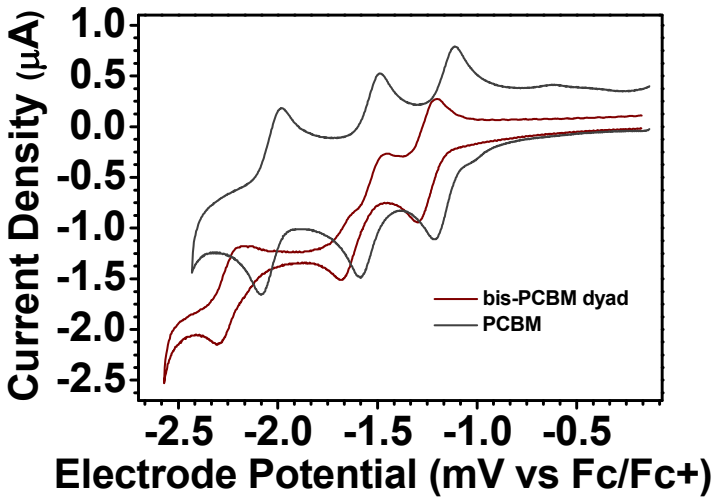

Figure 17. Cyclic voltammograms of PCBM and **bis-PCBM dyad** in *o*-DCB solution. Experimental conditions: values for $(E_{pa} + E_{pc})/2$ in V versus Fc/Fc^+; 10^{-4}–10^{-3} mol/L *o*-DCB solution; Bu_4NClO_4 (0.1 M) as supporting electrolyte; Pt wire as counter electrode; 50 mV/s scan rate.

4.2.4 Photovoltaic Effects

The fully optimization of the PSC device based on P3HT/**bis-PCBM dyad** is an extraordinarily time-consuming process since a complex region isomeric mixture of the bis-adduct has any negative side effects on the charge-transport properties.[46d] To demonstrate potential applications of the **bis-PCBM dyad** in PSCs, we used P3HT as an electron donor and **bis-PCBM dyad** as an electron acceptor. The blends were spin-coated from a mixture of solvents (chloroform/5% acetone) containing the P3HT/**bis-PCBM dyad** and subsequent thermal annealing 120 °C. The device architectures of the conventional and the inverted devices are ITO/PEDOT:PSS/P3HT:**bis-PCBM dyad** (1:1 w/w)/Al and ITO/TiO_x/ P3HT:**bis-PCBM dyad** (1:1 w/w)/MoO_3/Au, respectively. In the inverted devices, MoO_3 as the hole transport layer and TiO_x as the electron transport layer were deposited. The device structures of the regular and inverted polymer solar cells are shown in Figure 18a and b. All data were obtained under white light AM 1.5G illumination from a calibrated solar simulator with irradiation intensity of 100 mW/cm^2. The device performance of a solar cell is determined by the open-circuit voltage (V_{OC}), short-circuit current (J_{SC}), and fill factor (*FF*). The power conversion efficiency (η_e) of a solar cell is given as $\eta_e = (J_{SC} \cdot V_{OC} \cdot FF) \cdot 100 / P_{INC}$, where P_{INC} is the intensity of incident light. Higher values of those three parameters yield larger light-to-electricity power conversion efficiency. The PCE up to 0.76% is observed for the conventional P3HT:**bis-PCBM dyad** solar cells with a V_{OC} of 0.69 V, a short circuit current density (J_{SC}) of 3.05 mA/cm^2, and a fill factor (*FF*) of 36%. On the other hand, under the same white light illumination, the P3HT:**bis-PCBM dyad**-based inverted cells exhibit a J_{SC} of 1.06 mA/cm^2, a V_{OC} of 0.47 V, and a *FF* of 31%. It yields a substantially lower PCE of 0.16% because of its decreased photocurrent. Work is in progress in order to find optimal conditions for the PSCs based on P3HT/**bis-PCBM dyad**.

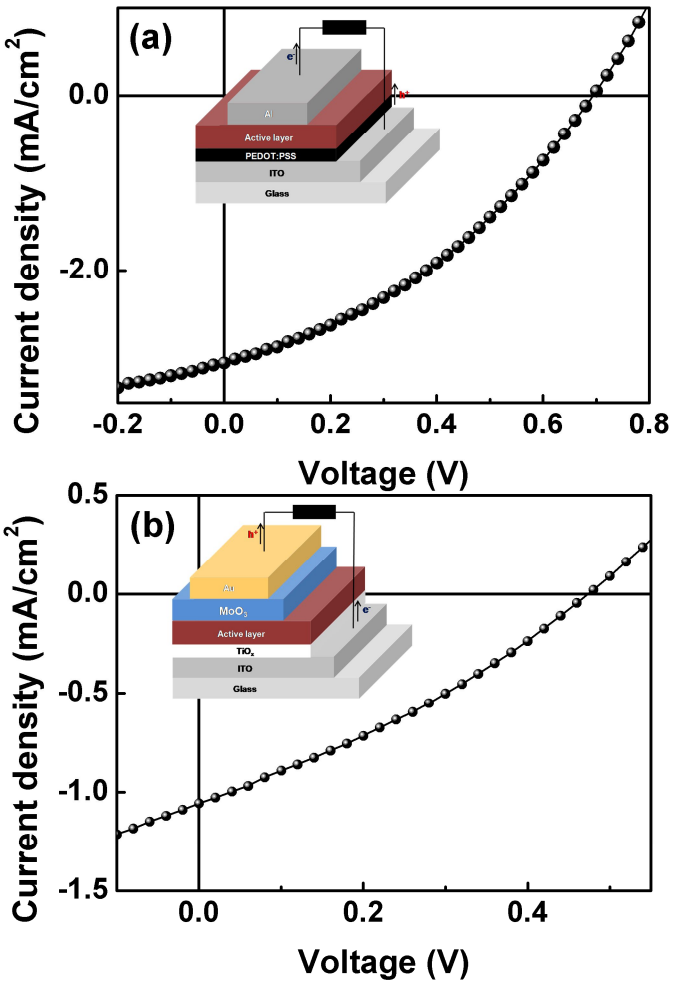

Figure 18. *J-V* characteristics of **bis-PCBM dyad** of conventional (a) and the inverted (b) devices under illumination of AM 1.5G, 100 mW/cm^2. Inset is a schematic of the device architectures of (a) and (b), respectively.

4.3 Conclusion

Aspiring to improve efficiency of the PSCs, we have presented a novel type of fullerene, **bis-PCBM dyad** bearing 4-nitro-α-cyanostilbene moieties, clearly identified through a combination of ^{1}H and ^{13}C NMR spectra. From the electrochemical and photophysical properties of the **bis-PCBM dyad**, one can conclude that the 4-nitro-α-cyanostilbene chromophores influence the absorption and electronic energy levels of the C_{60} derivatives very little. By virtue of 56 π-electron system in fullerene framework, the **bis-PCBM dyad** has a higher LUMO level and stronger absorption than PCBM, which should potentially be a highly helpful for minimizing the energy loss in the electron transfer from the donor to the acceptor material as well as increasing current generation in BHJ solar cells. By optimizing the device fabrication process, the photovoltaic performance of **bis-PCBM dyad** as acceptor blended with P3HT would be significantly superior to that of the traditional PCBM. As initial results, the efficiency obtained from the conventional structure device is 0.76%, while the PCE of the inverted device reaches 0.16%. Through successful device optimization of P3HT/**bis-PCBM dyad** cells, the high efficiency would be expected in the near future. Thus, future efforts will focus on testing the influence of **bis-PCBM dyad** in combination with P3HT on the performance of PSCs.

Chapter Ⅴ. Experimental Section

5.1 Materials

All starting materials were purchased either from Aldrich or Acros and used without further purification. All solvents are ACS grade unless otherwise noted. Anhydrous THF was obtained by distillation from sodium/benzophenone prior to use. Anhydrous toluene was used as received.

5.2 Instrumentations

^{1}H NMR and ^{13}C NMR spectra were recorded on a Varian VNMRS 600 spectrophotometer and MALDI MS spectra were obtained from Ultraflex III (Bruker, Germany). UV-Vis spectra were taken on Cary 5000 (Varian USA) spectrophotometer. Number-average (M_n) and weight-average (M_w) molecular weights, and polydispersity index (PDI) of the polymer products were determined by gel permeation chromatography (GPC) with Agilent 1200 HPLC Chemstation using a series of mono disperse polystyrene as standards in THF (HPLC grade) at 308 K. Cyclic voltammetry (CV) measurements were performed on AMETEK VersaSTAT 3 with a three-electrode cell in a nitrogen 0.1 M tetrabutylammonium perchlorate solution in *o*-DCB and 0.1 M tetra-*n*-butylammonium hexafluorophosphate (*n*-Bu_4NPF_6) in acetonitlie at a scan rate of 50 mV/s at room temperature. Ag used as the Ag/Ag^+ (0.1 M of $AgNO_3$ in acetonitrile) reference electrode, platinum counter electrode, and polymer coated platinum working electrode, respectively. The Ag/Ag^+ reference electrode was calibrated using a ferrocene/ferrocenium redox couple as an internal standard, whose oxidation potential is set at −4.8 eV with respect to zero vacuum level. The LUMO levels of polymers were obtained from the equation LUMO = − ($E_{red}^{onset} - E_{(ferrocene)}^{onset} + 4.8$) eV, $E_g^{opt} = 1240/\lambda_{edge}$, HOMO = − ($E_g^{opt}$ − LUMO) or HOMO = − ($E_{ox}^{onset} - E_{(ferrocene)}^{onset} + 4.8$) eV.

5.3 Synthesis of Poly[N-9′-heptadecanyl-2,7-carbazole-alt-5,5-(4′,7′-di-2-selenienyl-2,1,3-benzothiadiazole)]

Compounds **1, 2, 3,** and **4** were synthesized according to the previously reported procedures.[24a, 29]

Synthesis of 2,7-Bis(4′,4′,5′,5′-tetramethyl-1′,3′,2′-dioxaborolan-2′-yl)-N-9″-heptadecanylcarbazole (M1)

To a solution of compound **3** (1.5 g, 2.67 mmol) in anhydrous THF (50 mL) at the −78 °C, 1.6 M n-BuLi in hexane (4 mL) was added dropwise, the mixture being stirred at this temperature under Ar flow for 1 h, and 2- isopropoxy-4,4,5,5-tetramethyl-1,3,2-dioxaborolane (1.31 mL, 60.41 mmol) then being added. After 1h at −78 °C, the mixture was warmed to room temperature and stirred overnight. The mixture was poured into water, extracted with diethyl ether and dried over $MgSO_4$. The solvent was removed under reduced pressure, and the residue was purified by recrystallization in methanol/acetone (ca. 10:1) to give a title compound **M1** as a white crystal (1.37 g, Yield 79%). ^{1}H NMR (600 MHz, $CDCl_3$), δ (ppm): 8.14 (t, J = 7.2 Hz, 2H), 8.02 (s, 1H), 7.88 (s, 1H), 7.66 (br, 2H), 4.69 (m, 1H), 2.33 (m, 2H), 1.94 (m, 2H), 1.39 (br, 22H), 1.12 (br, 2H), 0.97 (m, 6H).

Synthesis of Tributyl(2-selenophenyl)stannane (5)

To a solution of selenophene (5.0 g, 38.17 mmol) in anhydrous THF (100 mL) at the −78 °C, 1.6 M n-BuLi in hexane (28.62 mL) was added dropwise, the mixture being stirred at this temperature under argon flow for 1 h, and tributylchlorostannane (11.05 mL, 41.0 mmol) then being added. The mixture was stirred at the −78 °C for 1.5 h and poured into saturated aqueous $NaHCO_3$. The organic phase was separated and washed with saturated aqueous brine and then dried over $MgSO_4$. The solvent was removed under reduced pressure, and the residue was purified by neutral alumina column chromatography (eluent hexane) to give a title compound **5** as colorless oil (12.43 g, Yield 77.5%). ^{1}H NMR (600 MHz, $CDCl_3$), δ (ppm): 8.36 (d, J = 4.8 Hz, 1H), 7.50 (m, 2H), 1.55 (m, 6H), 1.35 (m, 6H), 1.09 (m, 6H), 0.90 (t, 9H).

Synthesis of 4,7-Di(2′-selenienyl)-2,1,3-benzothiadiazole (6)

To a solution of 4,7-dibromo-2,1,3-benzothiadiazole (2.0 g, 6.0 mmol) and compound **5** (6.29 g, 14.9 mmol) in anhydrous toluene (40 mL) and anhydrous DMF (10 mL), $Pd(PPh_3)_4$ (0.4 g, 0.34 mmol) was added. The mixture was refluxed for 3 d. The solvent was removed under reduced pressure, and the residue was purified by silica gel column chromatography (eluent CH_2Cl_2/hexane, 1:1) to give a title compound **6** as a red solid (2.10 g, yield 78.4%). ^{1}H NMR (600 MHz, $CDCl_3$) δ (ppm): 8.19 (m, 4H), 7.91 (s, 2H), 7.45 (t, J = 3 Hz, 2H).

Synthesis of 4,7-Bis(5′-bromo-2′-selenienyl)-2,1,3-benzothiadiazole (M2)

To a solution of compound **6** (2.0 g, 5.07 mmol) in an anhydrous DMF (35 mL), N-bromosuccinimide (2.17 g, 12.17 mmol) was added, the mixture was stirred at room temperature under argon flow for 1 d and poured into water. The red precipitate was filtered off and washed with $NaHSO_4$ solution. Recrystallization from DMF twice gave a title compound **M2** as dark red solid (1.72 g, yield 51.6%). ^{1}H NMR (600 MHz, $CDCl_3$), δ (ppm): 7.87 (s, 2H), 7.79 (d, J = 4.8 Hz, 2H), 7.37 (d, J = 4.8 Hz, 2H).

Synthesis of Poly[*N*-9′-heptadecanyl-2,7-carbazole-alt-5,5-(4′,7′-di-2-selenienyl-2,1,3-benzothiadiazole)] (PCDSeBT)

In a flame-dried flask, **M1** (0.168 g, 0.30 mmol), **M2** (0.20 g, 0.30 mmol), tri-*o*-tolylposphine (P(*o*-Tol)$_3$, 7 mg, 0.024 mmol), K_3PO_4 (0.32 g, 1.52 mmol), and $Pd_2(dba)_3$ were dissolved in anhydrous toluene (8 mL) and deionized H_2O (2 mL). The mixture was stirred at the 90 °C under argon flow for 3days (end-capped with phenylboronic acid and bromobenzene). The solution was precipitated in a mixture of methanol and ammonia (4:1 v/v, 300 mL). The precipitate was filtered off and washed on Soxhlet apparatus with methanol, acetone, hexane, and chlorobenzene. The chlorobenzene fraction (150 − 200 mL) was reduced to 30 − 40 mL under reduced pressure precipitated into methanol (500 mL), filtered through 0.45 μm nylon filter and finally dried overnight under the vacuum. The dark violet polymer was obtained (130 mg, yield 52.4%, $M_n = 8.3 \times 10^4$ g/mol, $M_w = 2.0 \times 10^5$ g/mol, PDI = 2.51). ^{1}H NMR (600 MHz, $CDCl_3$). δ (ppm): 8.26 (br, 2H), 8.14 (br, 2H), 7.92 (br, 2H), 7.71 (br, 2H), 7.52 (br, 2H), 7.39 (br, 2H), 4.63 (br, 1H), 2.35 (br, 2H), 2.04 (br, 2H), 1.53 (br, 8H), 1.25 − 1.14 (br, 16H), 0.78 (br, 6H). Elemental Analysis. Calcd: C, 64.73; H, 6.19; N, 5.27; S, 4.02; Se, 19.79. Found: C, 64.37; H, 6.07; N, 5.22; S, 3.90.

5.4 Synthesis of TCZT and its polymers

Synthesis of *N*-9′-Heptadecanyl-2,7-dibromo-3,6-diiodocarbazole (7)

A mixture of *N*-9'-heptadecanyl-2,7-carbazole (**1**) (8 g, 14.20 mmol) and AcOH (130 mL) was heated to 80 °C, and then KI (6.27 g, 37.79 mmol) and KIO_3 (4.04 g, 18.89 mmol) were added in one portion. The mixture was stirred at 80 °C for 6 h and poured into water for extraction with CH_2Cl_2. The combined organic layers were washed with brine and dried over $MgSO_4$. After the solvent had been removed under reduced pressure, the residue was purified by recrystallization from alcohol to give a title compound **7** as a white solid (9.84 g, yield 84.05%). ^{1}H NMR (600 MHz, $CDCl_3$), δ (ppm): 8.49 (d, J = 21 Hz, 2H), 7.84 (s, 1H), 7.69 (s, 1H), 4.35 (m, 1H), 2.16 (m, 2H), 1.89 (m, 2H), 1.25 (br, 24H), 0.84 (m, 6H). ^{13}C NMR (150 MHz, $CDCl_3$): δ (ppm) 142.78, 139.19, 131.50, 131,27, 126.86, 126.31, 123.35, 121.98, 115.44, 113.24, 88.98, 88.60, 57.31, 33.39, 31.71, 29.23, 29.22, 29.08, 26.68, 26.65, 22.58, 14.07.

Synthesis of *N*-9′-Heptadecanyl-2,7-dibromo-3,6-di(trimetylsilyethyny)carbazole (8)

Into a Schlenk flask charged with $Pd(PPh_3)_2Cl_2$ (0.4 g, 0.58 mmol), CuI(0.11 g, 0.58 mmol), and compound **7** (9.5 g, 11.65 mmol) were added Et_3N (30 mL) and THF (30 mL). After addition of trimetylsilylacetylene (2.4 g, 24.47 mmol) dropwise, the mixture was stirred at room temperature for 48 h. The resulting yellow suspension was diluted with ethyl acetate. The organic layer was washed with saturated aqueous NH_4Cl solution and brine. After the solvent had been removed, the residue was purified by column chromatography on silica gel with hexane as eluent to give a title compound **8** as yellow oil (5.30 g , yield 60.2%). ^{1}H NMR (600 MHz, $CDCl_3$), δ (ppm): 8.17 (d, J = 13.8 Hz, 2H), 7.73 (s, 1H), 7.57 (s, 1H), 4.35 (m, 1H), 2.16 (m, 2H), 1.90 (m, 2H), 1.23 (br, 24H), 0.84 (m, 6H), 0.30 (m, 18H). ^{13}C NMR (150 MHz, $CDCl_3$): δ (ppm) 142.67, 139.24, 125.53, 125,39, 123.60, 122.99, 122.20, 120.80, 116.24, 115.35, 113.07, 97.56, 97.36, 57.35, 33.46, 31.72, 29.24, 29.20, 29.08, 26.64, 22.59, 14.06, 0.18, 0.00, −0.03, −0.18.

Synthesis of *N*-9′-Heptadecanyldithieno[2,3-*b*;7,6-*b*]carbazole (9)

To the suspension of $Na_2S{\cdot}9H_2O$ (6.1 g, 25.4 mmol) in NMP (100 mL) was added compound **8** (4.8 g, 6.35 mmol) and then stirred at 190 °C for 12 h. After being poured into saturated aqueous aqueous NH_4Cl solution, the mixture was extracted with Et_2O. The organic layer was washed with brine, dried over $MgSO_4$, and evaporated under reduced pressure. The crude product was purified by column chromatography on silica gel with hexane as eluent to give a title compound **9** as yellow oil (2.3 g, yield 69.8%). ^{1}H NMR (600 MHz, $CDCl_3$), δ (ppm): 8.57 [35a], 7.96 (s, 1H), 7.80 (s, 1H), 7.46 (d, J = 21 Hz, 2H), 7.33 (t, 2H), 4.58 (m, 1H), 2.37 (m, 2H), 1.98 (m, 2H), 1.24 (br, 24H), 0.80 (m, 6H). ^{13}C

NMR (150 MHz, $CDCl_3$): δ (ppm) 142.48, 139.04, 138.57, 132,58, 132.49, 123.72, 124.46, 123.06, 122.88, 122.22, 114.43, 114.18, 103.44, 100.86, 56.78, 33.29, 31.72, 29.42, 29.29, 29.23, 29.19, 29.13, 29.08, 26.87, 22.55, 14.05, 14.02.

Synthesis of *N*-9′-Heptadecanyl-3,8-bis(trimethylstannyl)dithieno[2,3-*b*;7,6-*b*]carbazole (TCZT)

At −78°C, into the solution of compound **9** (1.8 g, 3.47 mmol) in THF (40 mL) was added n-BuLi (5.42 mL, 8.67 mmol, 1.6 M in hexane) via syringe. The mixture was maintained at this temperature for 30 min, warmed to room temperature for another 1 h, and then recooled to −78 °C. Trimethyltin chloride (1.79 g, 9.02 mmol) was added at once. The mixture was stirred overnight at room temperature and poured into water for extraction with CH_2Cl_2. The combined organic layers were washed with aqueous $NaHCO_3$ solution and brine and dried over $MgSO_4$. After the solvent had been removed under reduced pressure, the residue was purified by recrystallization form hexane to give a title compound **TCZT** as a yellow solid (2.78 g, yield 95%). ^{1}H NMR (600 MHz, $CDCl_3$), δ (ppm): 8.54 (d, J = 21.6 Hz, 2H), 7.52 (s, 2H), 4.57 (m, 1H), 2.37 (m, 2H), 1.94 (m, 2H), 1.25 (br, 24H), 0.79 (m, 6H), 0.44 (m, 18H). ^{13}C NMR (150 MHz, $CDCl_3$): δ (ppm) 142.64, 142.17, 141.65, 137.66, 135.59, 135.35, 133.47, 133.37, 131.04, 122.69, 121.44, 112.61, 112.34, 102.01, 99.46, 55.80, 32.46, 30.93, 30.90, 28.62, 28.51, 28.33, 28.28, 25.98, 21.75, 13.26, -7.974, -8.026, -9.20, -10.37,-10.43.

General Synthesis Procedure of Polymers

Into a Schlenk flask charged with **TCZT**, count part compound, $Pd_2(dba)_3$ (2 mol%), and tri-o-tolylposphine (P(*o*-Tol)$_3$, 8 mol%) was degassed with argon, and then toluene was added. The mixture was further purged with argon 10 min and heated to 120 °C for 48 h (end-capped with bromobenzene and trimethyltinbenzene). The solution was precipitated in a mixture of methanol and ammonia (4:1 v/v, 300 mL). The precipitate was filtered off and washed on Soxhlet apparatus with methanol, acetone, hexane, and chloroform. The chloroform fraction (150 − 200 mL) was reduced to 30−40 mL under reduced pressure precipitated into methanol (500 mL), filtered through 0.45 μm nylon filter and finally dried overnight under the vacuum.

PTCZTBT TCZT (250 mg, 0.29 mmol), 4,7-dibromo-2,1,3-benzothiadiazole (87 mg, 0.29 mmol), the dark violet powder was obtained (147 mg, yield 78%, $M_n = 1.3 \times 10^4$ g/mol, $M_w = 1.9 \times 10^4$ g/mol, PDI = 1.45). ^{1}H NMR (600 MHz, $CDCl_3$), δ (ppm): δ 8.15–6.55 (br, 8H), 4.69–4.51 (br, 1H), 2.70–0.51 (br, 34H). Elemental Analysis. C, 71.84; H, 6.62; N, 6.44; S, 14.75; Found: C, 66.95; H, 6.49; N, 5.50; S, 11.61.

PTCZTfBT TCZT (250 mg, 0.29 mmol), 4,7-dibromo-5-fluoro-2,1,3-benzothiadiazole (92mg, 0.29 mmol), the violet powder was obtained (130 mg, yield 67%, $M_n = 4.4 \times 10^4$ g/mol, $M_w = 5.6 \times 10^4$ g/mol, PDI = 1.25). ^{1}H NMR (600 MHz, $CDCl_3$), δ (ppm): δ 8.46–6.70 (br, 7H), 4.60 (br, 1H), 2.88–0.81 (br, 34H). Elemental Analysis. C, 69.92; H, 6.62; N, 6.27; S, 14.36; Found: C, 64.43; H, 6.00; N, 5.64; S, 11.32.

PTCZTffBT TCZT (250 mg, 0.29 mmol), 4,7-dibromo-5,6-difluoro-2,1,3-benzothiadiazole (97 mg, 0.29 mmol), the violet powder was obtained (115 mg, yield 57.8%, $M_n = 3.4 \times 10^4$ g/mol, $M_w = 4.4 \times 10^4$ g/mol, PDI = 1.28). ^{1}H NMR (600 MHz, $CDCl_3$), δ (ppm): δ 8.37–6.69 (br, 6H), 4.56 (br, 1H), 2.89–0.94 (br, 34H). Elemental Analysis. C, 68.09; H, 6.30; N, 6.11; S, 13.98; Found: C, 63.47; H, 5.86; N, 5.53; S, 9.17.

PTCZTTT TCZT (352 mg, 4.17 mmol), 4,6-dibromo-1-prophanone-1-thieno[3,4-*b*]thiophene (148 mg, 4.17 mmol), the red powder was obtained (238 mg, yield 80.5%, $M_n = 1.1 \times 10^4$ g/mol, $M_w = 2.1 \times 10^4$ g/mol, PDI = 1.93). ^{1}H NMR (600 MHz, $CDCl_3$), δ (ppm): δ 8.01–7.08 (br, 7H), 4.60 (br, 1H), 3.36 (br, 2H), 2.40–0.82 (br, 37H). Elemental Analysis. C, 71.12; H, 7.08; N, 1.93; S, 17.66; O, 2.20; Found: C, 68.40; H, 7.12; N, 1.82; S, 14.48; O, 0.78.

PTCZTPT TCZT (200 mg, 0.23 mmol), 1,3-dibromo-5-octylthieno[3,4]pyrrol-4,6-dione (100 mg, 0.23 mmol), the dark green powder was obtained (150 mg, yield 83.8%, $M_n = 6.7 \times 10^4$ g/mol, $M_w = 1.9 \times 10^5$ g/mol, PDI = 2.83). ^{1}H NMR (600 MHz, $CDCl_3$), δ (ppm): δ 8.50–6.41 (br, 6H), 4.56 (br, 1H), 3.89 (br, 2H) 2.36–0.48 (br, 49H). Elemental Analysis. C, 77.37; H, 8.16; N, 3.87; S, 12.10; O, 4.02; Found: C, 69.84; H, 7.42; N, 3.46; S, 10.65; O, 4.18.

PTCZTQ TCZT (250 mg, 0.29 mmol), 5,8-dibromo-2,3-bis(octyloxy)phenylquinoxaline (206 mg, 0.29 mmol), the dark violet powder was obtained (280 mg, yield 91.8%, $M_n = 2.9 \times 10^4$ g/mol, $M_w = 4.0 \times 10^4$ g/mol, PDI = 1.35). ^{1}H NMR (600 MHz, $CDCl_3$), δ (ppm): δ 8.59–6.69 (br, 16H), 4.63 (br, 1H), 4.03–3.49 (br, 4H) 2.42–0.52 (br, 64H). Elemental Analysis. C, 78.58; H, 8.32; N, 3.93; S, 5.90; O, 2.94; Found: C, 73.99; H, 7.77; N, 3.68; S, 4.95; O, 1.86.

PTCZTfQ TCZT (118 mg, 0.14 mmol), 5,8-dibromo-6-fluoro-2,3-bis(octyloxy)phenylquinoxaline (100 mg, 0.14 mmol), the violet powder was obtained (130 mg, yield 89.4%, $M_n = 3.1 \times 10^4$ g/mol, $M_w = 5.1 \times 10^4$ g/mol, PDI = 1.33). ^{1}H NMR (600 MHz, $CDCl_3$), δ (ppm): δ 8.46–6.71 (br, 15H), 4.63 (br, 1H), 4.02–3.87 (br, 4H) 2.41–0.53 (br, 64H). Elemental Analysis. C, 77.27; H, 8.08; N, 3.92; S, 5.98; O, 2.98; Found: C, 73.52; H, 7.66; N, 3.64; S, 5.23; O, 2.98.

PTCZTffQ TCZT (115mg, 0.14 mmol), 5,8-dibromo-6,7-difluoro-2,3-bis(octyloxy)phenylquinoxaline (100 mg, 0.14 mmol), the violet powder was obtained (110 mg, yield 73.4%, $M_n = 1.1 \times 10^4$ g/mol, $M_w = 1.3 \times 10^4$ g/mol, PDI = 1.55). ^{1}H NMR (600 MHz, $CDCl_3$), δ (ppm): δ 8.60–6.94 (br, 14H), 4.61 (br, 1H), 4.01–3.87 (br, 4H) 2.41–0.54 (br, 64H). Elemental Analysis. C, 75.99; H, 7.86; N, 3.85; S, 5.88; O, 2.93; Found: C, 70.12; H, 7.23; N, 3.68; S, 5.66; O, 3.49.

5.5 Synthesis of bis-PCBM dyad

Synthesis of 4-nitro-4-hydroxy-a-cyanostilbene (10)

To a mixture of the 4-hydroxylbenezaldehyde (2.0 g, 16.39 mmol) and 4-nitrobenzylcyanide (2.66 g, 16.39 mmol) in absolute EtOH (40 mL), was added with piperidine (2.43 mL, 24.58 mmol) portionwise, stirred at room temperature for 3 h, cooled to 0 °C, and filtered. The precipitate was washed with EtOH, dried to yield **10** (95%). ^{1}H NMR (600 MHz, $CDCl_3$): d (ppm) 8.30 (d, J = 9 Hz, 2H), 7.92 (d, J = 8.4 Hz, 2H), 7.82 (d, J = 9 Hz, 2H), 7.60 (s, 1H), 6.98 (d, J = 8.4 Hz, 2H), 5.75 (s, 1H). ^{13}C NMR (150 MHz, acetone-d_6): δ (ppm) 161.50, 147.37, 145.81,141.52, 132.32, 126.36, 124.75, 123.92, 117.79. Elemental analysis: C, 67.67; H, 3.79; N, 10.52; O, 18.03; Found: C, 67.90; H, 3.89; N, 10.78; O, 18.15. Mp 204 °C. FTIR (n/ cm^{-1}): 3417, 2171, 1585, 1525, 1322.

Synthesis of bis-[6,6]-phenyl C61-butyric acid (bis-PCBA)

To a solution containing bis-PCBM (1.0 g, 0.90 mmol) in chlorobenzene was added acetic acid (70 mL) and concentrated HCl (20 mL). The mixture was heated to reflux overnight. The solvent was removed in vacuo and the precipitate was collected by filtration. The course of the reaction was followed by TLC (after complete conversion, Rf is 0.0). The crude product was washed with methanol and a solvent mixture of MeOH:diethylether (1:1 v/v) several times to give quantitative yield. Mp 302 °C. FTIR (n/cm^{-1}): 1711, 1438, 1421, 1210, 1190, 1157, 734, 573, 511.

Synthesis of bis-PCBM dyad

Compound **10** (0.18 g, 0.69 mmol) was mixed with bis-PCBA (0.17 g, 0.15 mmol) and 4-N,N-dimethylaminopyridine (DMAP) (0.4 g, 3.40 mmol) in *o*-DCB (60 mL). This mixture was treated in an ultrasonicator bath for 10 min, then cooled down to 0 °C in an ice/water bath. Finally, N,N-dicyclohexylcarbodiimide (DCC) (1.58 g, 7.65 mmol) was added to the mixture quickly with a syringe. The mixture was stirred at 0 °C for 5 h and then warmed up to room temperature with continuously stirring for 3 d. The mixture was concentrated to ca. 3 mL using a rotary evaporator, followed by addition of excess MeOH. The solid was separated by centrifugation (3000 rpm/30 min), washed with MeOH twice and then with diethyl ether twice, and further purified by column chromatography on silica gel with dichloromethane as eluent to yield **bis-PCBM dyad** (75%) as a dark red solid. ^{1}H NMR (600 MHz, $CDCl_3$): δ (ppm) 8.20-8.15 (m, 4H), 7.99-7.91 (m, 4H), 7.87-7.81 (m, 4H), 7.75-7.61 (m, 4H), 7.52-7.21 (m, 12H). ^{13}C NMR (150 MHz, $CDCl_3$): δ (ppm) 170.22, 149.94, 149.81, 149.21, 147.81, 146.75, 146.61, 146.45, 146.43, 146.40, 164.20, 146.12, 146.08, 146.00, 145.92, 145.84, 145.77, 145.39, 145.34, 145.23, 145.12, 144.99, 144.29 , 144.23, 144.07, 144.04, 143.88, 143.74, 143.16, 143.09, 142.81, 141.66, 141.50, 140.47, 140.26, 137.70, 137.56,

137.31, 136.89, 132.13, 131.90, 131.77, 128.30, 128.15, 128.02, 127.88, 127.85, 79.83, 79.25, 51.05, 51.00, 50.96, 49.48, 49.38, 33.92, 33.83, 33.77, 33.64, 33.18, 33.06, 32.60, 32.57, 30.78, 30.71, 30.64, 29.48, 26.28, 26.22, 25.30, 25.09, 24.54, 24.31, 22.52, 22.47, 22.41. Elemental Analysis: C, 85.71; H, 2.57; N, 3.57; O, 8.15; Found: C, 85.37; H, 2.34; N, 3.47; O, 8.12. MALDI-TOF-MS m/z: $[M]^{+\cdot}$= 1569. Mp 242 °C. FTIR (n/cm^{-1}): 2195, 1705, 1575, 1543, 1517, 1443, 1431, 1335, 1312, 1233, 1201, 1149, 701, 521.

5.6 Fabrication of conventional and inverted photovoltaic cells of bis-PCBM dyad

Two-type photovoltaic cells were fabricated on ITO-coated glass substrates. The ITO-coated glass substrates were first cleaned with detergent, ultrasonicated in water, acetone and isopropyl alcohol, and dried overnight in an oven. In conventional cells, PEDOT:PSS (Al 4083) was spin-cast on cleaned ITO substrates after a UV-ozone treatment for 15 min and heated at 140 °C for 10 min in air. Subsequently, the active layer was coated in a glove box. The solution containing a mixture of P3HT:**bis-PCBM dyad** (1:1 w/w) in a mixture of solvents (chloroform/5% acetone) with a concentration of 11 mg/mL and P3HT:**bis-PCBM dyad** (1:1) in a mixture of solvents (chloroform/5% acetone) with a concentration of 13 g/mL was spin-cast on top of PEDOT:PSS film. After then, the top electrode (Al) was deposited on the active layer in a vacuum ($<10^{-6}$ Torr) thermal evaporator. Inverted solar cells were fabricated on ITO-coated glass substrates. A TiO_x precursor solution was prepared using the sol-gel method. The TiO_x precursor solution was spin-cast on cleaned ITO substrates after a UV-ozone treatment for 15 min and heated at 80 °C for 10 min in air for conversion to TiO_x by hydrolysis. Subsequently, the TiO_x-coated substrates were transferred into a glove box. A solution containing a mixture of P3HT:**bis-PCBM dyad** (1:1 w/w) in a mixture of solvents (chloroform/5% acetone) was spin-cast on top of TiO_x films. Then, a thin layer of MoO_3 film (≅5 nm) was evaporated on top of the active layer. Finally, the anode (Au, ≅ 95 nm) was deposited on the active layer in a vacuum ($<10^{-6}$ Torr) thermal evaporator. The cross-sectional area of each of the electrode defines the active area of the device as 13.5 mm^2. Photovoltaic cell measurements were carried out inside the glove box using a high quality optical fiber to guide the light from the solar simulator equipped with a Keithley 2635A source measurement unit. The *J-V* curves for the devices were measured under AM 1.5G illumination at 100 mA/cm^2.

5.7 Fabrication of Photovoltaic Cells of PCDSeBT

Polymer solar cell devices were fabricated according to the following procedure: First, the ITO coated glass substrate was cleaned with detergent, then ultrasonicated in distilled water, acetone and isopropyl alcohol, and then dried overnight in an oven at the 100 °C. Poly(3,4-ethylenedioxythiophene):poly(styrenesulfonate) (PEDOT:PSS) (Baytron PH) was spin-cast at 5000 rpm for 40 s. The substrate was then dried for 10 min at the 140 °C in the air. Subsequently, it is moved into a glove box for spin-coating the active layer. A mixed solution of **PCDSeBT**:$PC_{71}BM$ in *o*-dichlorobenzene (*o*-DCB) was then spin coated at 700 rpm for 60s on top of the PEDOT:PSS layer to obtain a BHJ film. Those samples were brought into a vacuum system (about 10^{-7} Torr), and an Al electrode (100 nm) was deposited on top of the BHJ layer. Typical devices were thermally annealed in a Petri dish. Thermal annealing was carried out by directly placing the completed devices on a digitally controlled hot plate at 150 °C, in a glove box filled with nitrogen gas and after annealing. The devices were put on a metal plate and cooled to room temperature. Measurements were carried out with the solar cells inside the glove box by using a high quality optical fiber to guide the light from the solar simulator equipped with a Keithley 2635 A source. The solar cell devices were illuminated at an intensity of 100 mW/cm^2. For more accurate information the IPCE measurements were carried out with QEX7. The device structure of the hole and electron only devices are ITO/PEDOT:PSS/**PCDSeBT**:$PC_{71}BM$/Au and FTO/**PCDSeBT**:$PC_{71}BM$/Al, respectively. The space-charge-limited current (SCLC) mobilities were estimated the Mott-Gurney square law $J_{SCLC} = 9/8 \times \varepsilon_r\varepsilon_0 \times \mu(V^2/L^3)$, where ε_r is the dielectric constant of the material, ε_0 is the permittivity of free space, L is the distance between the cathode and anode, which is equivalent to the film thickness, and V is the applied voltage.

5.8 OFET Device Preparation and Measurement of PCDSeBT

Highly doped n^+-Si wafers were used as substrates, and a layer of 200 nm of silicon dioxide (SiO_2:grown by thermal oxidation) was used as the gate dielectric layer. Au (60 nm) was successively evaporated with shadow mask to obtain source and drain electrodes. The interdigitated structure of the source-drain contacts determined a channel length of 50 μm and a channel width of 2950 μm. Substrates were cleaned by acetone, isopropanol and dried at 100 °C oven for 20 min, and treated with octadecyltrichlorosilane (OTS) at room temperature for over 12 h to treat the surface. Organic semiconductor layers (60 nm) were deposited by spin-coating at 1500 rpm. All fabrication processes were carried out in a glove box filled with N_2. Electrical characterization was performed using a Keithley semiconductor parametric analyzer (Keithley 4200-SCS) under N_2 atmosphere. The electron mobility (μ) was determined using the following equation in the saturation regime; $I_{ds} = (WC_i/2L) \times \mu \times (V_{gs} - V_{Th})^2$, where C_i is the capacitance per unit area of the SiO_2 dielectric (C_i = 15 nF/cm^2) and V_{Th} is the threshold voltage.

Chapter Ⅵ. References

1. Marks, R. N.; Halls, J. J. M.; Bradley, D. D. C.; Friend, R. H.; Holmes, A. B., The photovoltaic response in poly(p-phenylene vinylene) thin-film devices. *Adv. Funct. Mater.* **1994,** *6* (7), 1379-1394.
2. Halls, J. J. M.; Walsh, C. A.; Greenham, N. C.; Marseglla, E. A.; Friend, R. H.; Moratti, S. C.; Holmes, A. B., Efficient photodiodes from interpenetrating polymer networks. *Nature* **1995,** *376* (6540), 498-500.
3. Yamamoto, T., π-conjugated polymers with electronic and optical functionalities: Preparation by organometallic polycondensation, properties, and applications. *Macromol. Rapid Commun.* **2002,** *23* (10-11), 583-606.
4. Li, G. Y., Highly active, air-stable palladium catalysts for Kumada-Tamao-Corriu cross-coupling reaction of inactivated aryl chlorides with aryl Grignard reagents. *J. Organ. Chem.* **2002,** *653* (1-2), 63-68.
5. Echavarren, A. M.; Cárdenas, D. J., Mechanistic Aspects of Metal-Catalyzed C,C- and C,X-Bond-Forming Reactions. In *Metal-Catalyzed Cross-Coupling Reactions*, Wiley-VCH Verlag GmbH: 2008; pp 1-40.
6. Heck, R. F., Palladium-Catalyzed Vinylation of Organic Halides. In *Organic Reactions*, John Wiley & Sons, Inc.: 2004.
7. Martin, R.; Buchwald, S. L., Palladium-Catalyzed Suzuki−Miyaura Cross-Coupling Reactions Employing Dialkylbiaryl Phosphine Ligands. *Acc. Chem. Res.* **2008,** *41* (11), 1461-1473.
8. Bao, Z.; Chan, W. K.; Yu, L., Exploration of the Stille coupling reaction for the syntheses of functional polymers. *J. Am. Chem. Soc.* **1995,** *117* (50), 12426-12435.
9. Tykwinski, R. R., Evolution in the palladium-catalyzed cross-coupling of sp- and sp2-hybridized carbon atoms. *Angew. Chem. Int. Ed.* **2003,** *42* (14), 1566-1568.
10. Denmark, S. E.; Sweis, R. F., Design and implementation of new, silicon-based, cross-coupling reactions: Importance of silicon-oxygen bonds. *Acc. Chem. Res.* **2002,** *35* (10), 835-846.
11. Fanta, P. E., The Ullmann Synthesis of Biaryls, 1945-1963. *Chem. Rev.* **1964,** *64* (6), 613-632.
12. Gibtner, T.; Hampel, F.; Gisselbrecht, J. P.; Hirsch, A., End-cap stabilized oligoynes: Model compounds for the linear sp carbon allotrope carbyne. *Chem. Eur. J.* **2002,** *8* (2), 408-432.
13. Kubo, M.; Takimoto, C.; Minami, Y.; Uno, T.; Itoh, T.; Shoyama, M., Incorporation of π-conjugated polymer into silica: Preparation of poly[2-methoxy-5-(2-ethylhexyloxy)-1,4-phenylenevinylene]/silica and poly(3-hexylthiophene)/silica composites. *Macromolecules*

2005, *38* (17), 7314-7320.

14. Greenham, N. C.; Moratti, S. C.; Bradley, D. D. C.; Friend, R. H.; Holmes, A. B., Efficient light-emitting diodes based on polymers with high electron affinities. *Nature* **1993,** *365* (6447), 628-630.
15. Sariciftci, N. S.; Smilowitz, L.; Heeger, A. J.; Wudl, F., Photoinduced electron transfer from a conducting polymer to buckminsterfullerene. *Science* **1992,** *258* (5087), 1474-1476.
16. (a) Backer, S. A.; Sivula, K.; Kavulak, D. F.; Fréchet, J. M. J., High efficiency organic photovoltaics incorporating a new family of soluble fullerene derivatives. *Chem. Mater.* **2007,** *19* (12), 2927-2929; (b) Popescu, L. M.; Van 'T Hof, P.; Sieval, A. B.; Jonkman, H. T.; Hummelen, J. C., Thienyl analog of 1-(3-methoxycarbonyl)propyl-1-phenyl-[6,6]-methanofullerene for bulk heterojunction photovoltaic devices in combination with polythiophenes. *Appl. Phys. Lett.* **2006,** *89* (21).
17. (a) Cheedarala, R. K.; Kim, G. H.; Cho, S.; Lee, J.; Kim, J.; Song, H. K.; Kim, J. Y.; Yang, C., Ladder-type heteroacene polymers bearing carbazole and thiophene ring units and their use in field-effect transistors and photovoltaic cells. *J. Mater. Chem.* **2011,** *21* (3), 843-850; (b) Li, G.; Shrotriya, V.; Huang, J.; Yao, Y.; Moriarty, T.; Emery, K.; Yang, Y., High-efficiency solution processable polymer photovoltaic cells by self-organization of polymer blends. *Nature Mater.* **2005,** *4* (11), 864-868; (c) Yang, C.; Jin, Y. K.; Cho, S.; Jae, K. L.; Heeger, A. J.; Wudl, F., Functionalized methanofullerenes used as n-type materials in bulk-heterojunction polymer solar cells and in field-effect transistors. *J. Am. Chem. Soc.* **2008,** *130* (20), 6444-6450.
18. (a) Kooistra, F. B.; Knol, J.; Kastenberg, F.; Popescu, L. M.; Verhees, W. J. H.; Kroon, J. M.; Hummelen, J. C., Increasing the open circuit voltage of bulk-heterojunction solar cells by raising the LUMO level of the acceptor. *Org. Lett.* **2007,** *9* (4), 551-554; (b) Xu, Z.; Chen, L. M.; Yang, G.; Huang, C. H.; Hou, J.; Wu, Y.; Li, G.; Hsu, C. S.; Yang, Y., Vertical phase separation in poly(3-hexylthiophene): Fullerene derivative blends and its advantage for inverted structure solar cells. *Adv. Funct. Mater.* **2009,** *19* (8), 1227-1234.
19. (a) Choi, J. H.; Son, K. I.; Kim, T.; Kim, K.; Ohkubo, K.; Fukuzumi, S., Thienyl-substituted methanofullerene derivatives for organic photovoltaic cells. *J. Mater. Chem.* **2010,** *20* (3), 475-482; (b) Huang, F.; Chen, K. S.; Yip, H. L.; Hau, S. K.; Acton, O.; Zhang, Y.; Luo, J.; Jen, A. K. Y., Development of new conjugated polymers with donor-π-bridge-acceptor side chains for high performance solar cells. *J. Am. Chem. Soc.* **2009,** *131* (39), 13886-13887; (c) Troshin, P. A.; Hoppe, H.; Renz, J.; Egginger, M.; Mayorova, J. Y.; Goryachev, A. E.; Peregudov, A. S.; Lyubovskaya, R. N.; Gobsch, G.; Sariciftci, N. S.; Razumov, V. F., Material solubility-photovoltaic performance relationship in the design of novel fullerene derivatives for bulk

heterojunction solar cells. *Adv. Funct. Mater.* **2009,** *19* (5), 779-788; (d) Zhang, Y.; Yip, H. L.; Acton, O.; Hau, S. K.; Huang, F.; Jen, A. K. Y., A simple and effective way of achieving highly efficient and thermally stable bulk-heterojunction polymer solar cells using amorphous fullerene derivatives as electron acceptor. *Chem. Mater.* **2009,** *21* (13), 2598-2600; (e) Zhao, H.; Guo, X.; Tian, H.; Li, C.; Xie, Z.; Geng, Y.; Wang, F., Alkyl substituted [6,6]-thienyl-C 61-butyric acid methyl esters: Easily accessible acceptor materials for bulk-heterojunction polymer solar cells. *J. Mater. Chem.* **2010,** *20* (15), 3092-3097.

20. (a) Imahori, H.; Tamaki, K.; Guldi, D. M.; Luo, C.; Fujitsuka, M.; Ito, O.; Sakata, Y.; Fukuzumi, S., Modulating charge separation and charge recombination dynamics in porphyrin-fullerene linked dyads and triads: Marcus-normal versus inverted region. *J. Am. Chem. Soc.* **2001,** *123* (11), 2607-2617; (b) Thilgen, C.; Diederich, F., Structural aspects of fullerene chemistry - A journey through fullerene chirality. *Chem. Rev.* **2006,** *106* (12), 5049-5135.

21. Ma, W.; Yang, C.; Gong, X.; Lee, K.; Heeger, A. J., Thermally stable, efficient polymer solar cells with nanoscale control of the interpenetrating network morphology. *Adv. Funct. Mater.* **2005,** *15* (10), 1617-1622.

22. Peet, J.; Kim, J. Y.; Coates, N. E.; Ma, W. L.; Moses, D.; Heeger, A. J.; Bazan, G. C., Efficiency enhancement in low-bandgap polymer solar cells by processing with alkane dithiols. *Nature Mater.* **2007,** *6* (7), 497-500.

23. Coffin, R. C.; Peet, J.; Rogers, J.; Bazan, G. C., Streamlined microwave-assisted preparation of narrow-bandgap conjugated polymers for high-performance bulk heterojunction solar cells. *Nature Chem.* **2009,** *1* (8), 657-661.

24. (a) Blouin, N.; Michaud, A.; Leclerc, M., A low-bandgap poly(2,7-carbazole) derivative for use in high-performance solar cells. *Adv. Mater.* **2007,** *19* (17), 2295-2300; (b) Park, S. H.; Roy, A.; Beaupré, S.; Cho, S.; Coates, N.; Moon, J. S.; Moses, D.; Leclerc, M.; Lee, K.; Heeger, A. J., Bulk heterojunction solar cells with internal quantum efficiency approaching 100%. *Nature Photon.* **2009,** *3* (5), 297-303; (c) Cho, S.; Seo, J. H.; Park, S. H.; Beaupré, S.; Leclerc, M.; Heeger, A. J., A thermally stable semiconducting polymer. *Adv. Mater.* **2010,** *22* (11), 1253-1257.

25. (a) Alem, S.; Chu, T. Y.; Tse, S. C.; Wakim, S.; Lu, J.; Movileanu, R.; Tao, Y.; Bélanger, F.; Désilets, D.; Beaupré, S.; Leclerc, M.; Rodman, S.; Waller, D.; Gaudiana, R., Effect of mixed solvents on PCDTBT:PC 70BM based solar cells. *Org. Electron.* **2011,** *12* (11), 1788-1793; (b) Moon, J. S.; Jo, J.; Heeger, A. J., Nanomorphology of PCDTBT:PC 70BM bulk heterojunction solar cells. *Adv. Energy Mater.* **2012,** *2* (3), 304-308.

26. (a) Wu, J. S.; Cheng, Y. J.; Dubosc, M.; Hsieh, C. H.; Chang, C. Y.; Hsu, C. S., Donor-

acceptor polymers based on multi-fused heptacyclic structures: Synthesis, characterization and photovoltaic applications. *Chem. Commun.* **2010,** *46* (19), 3259-3261; (b) Cheng, Y. J.; Wu, J. S.; Shih, P. I.; Chang, C. Y.; Jwo, P. C.; Kao, W. S.; Hsu, C. S., Carbazole-based ladder-type heptacylic arene with aliphatic side chains leading to enhanced efficiency of organic photovoltaics. *Chem. Mater.* **2011,** *23* (9), 2361-2369.

27. Heeney, M.; Zhang, W.; Crouch, D. J.; Chabinyc, M. L.; Gordeyev, S.; Hamilton, R.; Higgins, S. J.; McCulloch, I.; Skabara, P. J.; Sparrowe, D.; Tierney, S., Regioregular poly(3-hexyl)selenophene: A low band gap organic hole transporting polymer. *Chem. Commun.* **2007,** (47), 5061-5063.
28. Patra, A.; Bendikov, M., Polyselenophenes. *J. Mater. Chem.* **2010,** *20* (3), 422-433.
29. Yang, R.; Tian, R.; Yan, J.; Zhang, Y.; Yang, J.; Hou, Q.; Yang, W.; Zhang, C.; Cao, Y., Deep-red electroluminescent polymers: Synthesis and characterization of new low-band-gap conjugated copolymers for light-emitting diodes and photovoltaic devices. *Macromolecules* **2005,** *38* (2), 244-253.
30. Yamamoto, T.; Takimiya, K., Facile synthesis of highly π-extended heteroarenes, dinaphtho[2,3-b: 2′,3′-f]chalcogenopheno[3,2-b]chalcogenophenes, and their application to field-effect transistors. *J. Am. Chem. Soc.* **2007,** *129* (8), 2224-2225.
31. (a) Dennler, G.; Scharber, M. C.; Brabec, C. J., Polymer-fullerene bulk-heterojunction solar cells. *Adv. Mater.* **2009,** *21* (13), 1323-1338; (b) Zade, S. S.; Bendikov, M., From oligomers to polymer: Convergence in the HOMO-LUMO gaps of conjugated oligomers. *Org. Lett.* **2006,** *8* (23), 5243-5246.
32. Wang, E.; Hou, L.; Wang, Z.; Hellström, S.; Zhang, F.; Inganäs, O.; Andersson, M. R., An easily synthesized blue polymer for high-performance polymer solar cells. *Adv. Mater.* **2010,** *22* (46), 5240-5244.
33. Wienk, M. M.; Turbiez, M.; Gilot, J.; Janssen, R. A. J., Narrow-bandgap diketo-pyrrolo-pyrrole polymer solar cells: The effect of processing on the performance. *Adv. Mater.* **2008,** *20* (13), 2556-2560.
34. (a) Kronemeijer, A. J.; Gili, E.; Shahid, M.; Rivnay, J.; Salleo, A.; Heeney, M.; Sirringhaus, H., A selenophene-based low-bandgap donor-acceptor polymer leading to fast ambipolar logic. *Adv. Mater.* **2012,** *24* (12), 1558-1565; (b) Shahid, M.; McCarthy-Ward, T.; Labram, J.; Rossbauer, S.; Domingo, E. B.; Watkins, S. E.; Stingelin, N.; Anthopoulos, T. D.; Heeney, M., Low band gap selenophene-diketopyrrolopyrrole polymers exhibiting high and balanced ambipolar performance in bottom-gate transistors. *Chem. Sci.* **2012,** *3* (1), 181-185.
35. (a) Chattopadhyaya, M.; Sen, S.; Alam, M. M.; Chakrabarti, S., *J. Chem. Phys.* **2012,** *136*, 094904; (b) Patra, A.; Wijsboom, Y. H.; Leitus, G.; Bendikov, M., Tuning the band gap of

low-band-gap polyselenophenes and polythiophenes: The effect of the heteroatom. *Chem. Mater.* **2011,** *23* (3), 896-906; (c) Zade, S. S.; Zamoshchik, N.; Bendikov, M., *Acc. Chem. Res.* **2010,** *44*.

36. Scharber, M. C.; Mühlbacher, D.; Koppe, M.; Denk, P.; Waldauf, C.; Heeger, A. J.; Brabec, C. J., Design rules for donors in bulk-heterojunction solar cells - Towards 10 % energy-conversion efficiency. *Adv. Mater.* **2006,** *18* (6), 789-794.
37. Li, J.; Grimsdale, A. C., Carbazole-based polymers for organic photovoltaic devices. *Chem. Soc. Rev.* **2010,** *39* (7), 2399-2410.
38. Chu, T. Y.; Alem, S.; Tsang, S. W.; Tse, S. C.; Wakim, S.; Lu, J.; Dennler, G.; Waller, D.; Gaudiana, R.; Tao, Y., *Appl. Phys. Lett.* **2011,** *98*, 253301.
39. Saadeh, H. A.; Lu, L.; He, F.; Bullock, J. E.; Wang, W.; Carsten, B.; Yu, L., *ACS Macro Lett.* **2012,** *1*, 361-365.
40. (a) Gao, J.; Li, R.; Li, Q.; Meng, Q.; Jiang, H.; Li, H.; Hu, W., High-performance field-effect transistor based on dibenzo[d,d′] thieno[3,2-b;4,5-6′]dithiophene, an easily synthesized semiconductor with high ionization potential. *Adv. Mater.* **2007,** *19* (19), 3008-3011; (b) Gao, P.; Beckmann, D.; Tsao, H. N.; Feng, X.; Enkelmann, V.; Baumgarten, M.; Pisula, W.; Müllen, K., Dithieno[2,3-d;2′3′-d′]benzo[1,2-b;4,5-b′] dithiophene (DTBDT) as semiconductor for high-performance, solution-processed organic field-effect transistors. *Adv. Mater.* **2009,** *21* (2), 213-216; (c) Izawa, T.; Miyazaki, E.; Takimiya, K., Molecular ordering of high-performance soluble molecular semiconductors and re-evaluation of their field-effect transistor characteristics. *Adv. Mater.* **2008,** *20* (18), 3388-3392; (d) Kelley, T. W.; Muyres, D. V.; Baude, P. F.; Smith, T. P.; Jones, T. D., *Mater. Res. Soc. Symp. Proc.* **2003,** *771*.
41. (a) Jiang, Y.; Okamoto, T.; Becerril, H. A.; Hong, S.; Tang, M. L.; Mayer, A. C.; Parmer, J. E.; McGehee, M. D.; Bao, Z., Anthradithiophene-containing copolymers for thin-film transistors and photovoltaic cells. *Macromolecules* **2010,** *43* (15), 6361-6367; (b) Okamoto, T.; Bao, Z., Synthesis of solution-soluble pentacene-containing conjugated copolymers. *J. Am. Chem. Soc.* **2007,** *129* (34), 10308-10309; (c) Okamoto, T.; Jiang, Y.; Qu, F.; Mayer, A. C.; Farmer, J. E.; McGehee, M. D.; Bao, Z., Synthesis and characterization of pentacene- and anthradithiophene-fluorene conjugated copolymers synthesized by suzuki reactions. *Macromolecules* **2008,** *41* (19), 6977-6980.
42. (a) Blouin, N.; Leclerc, M., Poly(2,7-carbazole)s: Structure-property relationships. *Acc. Chem. Res.* **2008,** *41* (9), 1110-1119; (b) Liu, P.; Wu, Y.; Pan, H.; Ong, B. S.; Zhu, S., High-performance polythiophene thin-film transistors processed with environmentally benign solvent. *Macromolecules* **2010,** *43* (15), 6368-6373; (c) Morin, J. F.; Leclere, M.; Adès, D.; Siove, A., Polycarbazoles: 25 years of progress. *Macromol. Rapid Commun.* **2005,** *26* (10),

761-778; (d) Zhang, Q.; Chen, J.; Cheng, Y.; Wang, L.; Ma, D.; Jing, X.; Wang, F., Novel hole-transporting materials based on 1,4-bis(carbazolyl)benzene for organic light-emitting devices. *J. Mater. Chem.* **2004,** *14* (5), 895-900.

43. (a) Hummelen, J. C.; Knight, B. W.; Lepeq, F.; Wudl, F.; Yao, J.; Wilkins, C. L., Preparation and characterization of fulleroid and methanofullerene derivatives. *J. Org. Chem.* **1995,** *60* (3), 532-538; (b) Janssen, R. A. J.; Christiaans, M. P. T.; Pakbaz, K.; Moses, D.; Hummelen, J. C.; Sariciftci, N. S., Photoinduced electron transfer processes in oligothiophene/C60 composite films. *J. Chem. Phys.* **1995,** *102* (6), 2628-2635; (c) Yu, G.; Gao, J.; Hummelen, J. C.; Wudl, F.; Heeger, A. J., Polymer photovoltaic cells: Enhanced efficiencies via a network of internal donor-acceptor heterojunctions. *Science* **1995,** *270* (5243), 1789-1791.

44. Padinger, F.; Rittberger, R. S.; Sariciftci, N. S., Effects of postproduction treatment on plastic solar cells. *Adv. Funct. Mater.* **2003,** *13* (1), 85-88.

45. (a) Kim, J.; Yun, M. H.; Lee, J.; Kim, J. Y.; Wudl, F.; Yang, C., A synthetic approach to a fullerene-rich dendron and its linear polymer via ring-opening metathesis polymerization. *Chem. Commun.* **2011,** *47* (11), 3078-3080; (b) Zhao, G.; He, Y.; Xu, Z.; Hou, J.; Zhang, M.; Min, J.; Chen, H. Y.; Ye, M.; Hong, Z.; Yang, Y.; Li, Y., Effect of carbon chain length in the substituent of PCBM-like molecules on their photovoltaic properties. *Adv. Funct. Mater.* **2010,** *20* (9), 1480-1487.

46. (a) He, Y.; Chen, H. Y.; Hou, J.; Li, Y., Indene - C60 bisadduct: A new acceptor for high-performance polymer solar cells. *J. Am. Chem. Soc.* **2010,** *132* (4), 1377-1382; (b) Kang, H.; Cho, C. H.; Cho, H. H.; Kang, T. E.; Kim, H. J.; Kim, K. H.; Yoon, S. C.; Kim, B. J., Controlling number of indene solubilizing groups in multiadduct fullerenes for tuning optoelectronic properties and open-circuit voltage in organic solar cells. *ACS Appl. Mater. Interfaces* **2012,** *4* (1), 110-116; (c) Kim, K. H.; Kang, H.; Nam, S. Y.; Jung, J.; Kim, P. S.; Cho, C. H.; Lee, C.; Yoon, S. C.; Kim, B. J., Facile synthesis of o-xylenyl fullerene multiadducts for high open circuit voltage and efficient polymer solar cells. *Chem. Mater.* **2011,** *23* (22), 5090-5095; (d) Lenes, M.; Wetzelaer, G. J. A. H.; Kooistra, F. B.; Veenstra, S. C.; Hummelen, J. C.; Blom, P. W. M., Fullerene bisadducts for enhanced open-circuit voltages and efficiencies in polymer solar cells. *Adv. Mater.* **2008,** *20* (11), 2116-2119; (e) Zhao, G. J.; He, Y. J.; Li, Y., 6.5% efficiency of polymer solar cells based on poly(3-hexylthiophene) and indene-C 60 bisadduct by device optimization. *Adv. Mater.* **2010,** *22* (39), 4355-4358.

47. (a) Kim, G.; Yeom, H. R.; Cho, S.; Seo, J. H.; Kim, J. Y.; Yang, C., Easily attainable phenothiazine-based polymers for polymer solar cells: Advantage of insertion of S,S-dioxides into its polymer for inverted structure solar cells. *Macromolecules* **2012,** *45* (4), 1847-1857;

(b) Kim, J.; Yun, M. H.; Anant, P.; Cho, S.; Jacob, J.; Kim, J. Y.; Yang, C., Copolymers comprising 2,7-carbazole and bis-benzothiadiazole units for bulk-heterojunction solar cells. *Chem. Eur. J.* **2011,** *17* (51), 14681-14688; (c) Lee, J.; Yun, M. H.; Kim, J.; Kim, J. Y.; Yang, C., Toward the realization of A practical diketopyrrolopyrrole-based small molecule for improved efficiency in ternary BHJ solar cells. *Macromol. Rapid Commun.* **2012,** *33* (2), 140-145; (d) Wienk, M. M.; Kroon, J. M.; Verhees, W. J. H.; Knol, J.; Hummelen, J. C.; Van Hal, P. A.; Janssen, R. A. J., Efficient methano[70]fullerene/MDMO-PPV bulk heterojunction photovoltaic cells. *Angew. Chem., Int. Ed. Engl.* **2003,** *42* (29), 3371-3375; (e) Yun, M. H.; Kim, G. H.; Yang, C.; Kim, J. Y., Towards optimization of P3HT:bisPCBM composites for highly efficient polymer solar cells. *J. Mater. Chem.* **2010,** *20* (36), 7710-7714.

48. (a) Gómez, R.; Segura, J. L.; Martín, N., Highly efficient light-harvesting organofullerenes. *Org. Lett.* **2005,** *7* (4), 717-720; (b) Martín, N.; Sánchez, L.; Illescas, B.; Pérez, I., C60-based electroactive organofullerenes. *Chem. Rev.* **1998,** *98* (7), 2527-2547; (c) Segura, J. L.; Gómez, R.; Martin, N.; Luo, C.; Guldi, D. M., Competition between photosensitization and charge transfer in soluble oligo(naphthylenevinylene)-fullerene dyads. *Chem. Commun.* **2000,** (8), 701-702; (d) Segura, J. L.; Martín, N., Molecular triads of soluble oligo-2,6-naphthylenevinylenes end-capped with [60]fullerene. *Tetrahedron Lett.* **1999,** *40* (16), 3239-3242.

49. Mikroyannidis, J. A.; Kabanakis, A. N.; Sharma, S. S.; Sharma, G. D., A simple and effective modification of PCBM for use as an electron acceptor in efficient bulk heterojunction solar cells. *Adv. Funct. Mater.* **2011,** *21* (4), 746-755.

50. Mikroyannidis, J. A.; Tsagkournos, D. V.; Balraju, P.; Sharma, G. D., Simple sensitizers of low band gap based on 4-nitro-a-cyanostilbene prepared from a one-step reaction for efficient dye-sensitized solar cells. *Org. Electron.* **2010,** *11* (7), 1242-1249.

51. (a) Neises, B.; Steglich, W., Simple method for the esterification of carboxylic acids. *Angew. Chem., Int. Ed. Engl.* **1978,** *17*, 522-524; (b) Wang, M.; Heeger, A. J.; Wudl, F., Self-assembly of a fullerene poly(3-hexylthiophene) dyad. *Small* **2011,** *7* (3), 298-301.

52. (a) Brites, M. J.; Santos, C.; Nascimento, S.; Gigante, B.; Luftmann, H.; Fedorov, A.; Berberan-Santos, M. N., Synthesis and fluorescence properties of [60] and [70]fullerene-coumarin dyads: Efficient dipole-dipole resonance energy transfer from coumarin to fullerene. *New J. Chem.* **2006,** *30* (7), 1036-1045; (b) Liu, Y.; Zhao, J., Visible light-harvesting perylenebisimide-fullerene (C 60) dyads with bidirectional "ping-pong" energy transfer as triplet photosensitizers for photooxidation of 1,5-dihydroxynaphthalene. *Chem. Commun.* **2012,** *48* (31), 3751-3753.

53. (a) Kordatos, K.; Da Ros, T.; Prato, M.; Bensasson, R. V.; Leach, S., Absorption spectra of the

mono-adduct and eight bis-adduct regioisomers of pyrrolidine derivatives of C60. *Chem. Phys.* **2003,** *293* (2), 263-280; (b) Meng, X.; Zhang, W.; Tan, Z.; Li, Y.; Ma, Y.; Wang, T.; Jiang, L.; Shu, C.; Wang, C., Highly efficient and thermally stable polymer solar cells with dihydronaphthyl-based [70]fullerene bisadduct derivative as the acceptor. *Adv. Funct. Mater.* **2012,** *22* (10), 2187-2193.

- Chapter Ⅱ is introduced from my paper of "A Selenophene Analogue of PCDTBT: Selective Fine-Tuning of LUMO to Lower of the Bandgap for Efficient Polymer Solar Cells".
- Chapter Ⅳ is introduced from my paper of "Synthesis and characterization of a bis-methanofullerene-4-nitro-α-cyanostilbene dyad as a potential acceptor for high-performance polymer solar cells".

Chapter Ⅶ. Summary and Outlook

We synthesized and characterized poly(2,7-carbazole-*alt*-diselenienylbenzothiadiazole) (**PCDSeBT**) by replacing thiophenes with selenophene rings in the polymer backbone, **bis-PCBM dyad** containing 4-nitro-a-cyanostilbene units, and eight alternating conjugate polymers comprising a S- and N-containing heteroarene, i.e, *N*-9′-Heptadecanyldithieno[2,3-*b*;7,6-*b*]carbazole (**PTCZTBT**, **PTCZTfBT**, **PTCZTffBT, PTCZTTT**, **PTCZTPT**, **PTCZTQ**, **PTCZTfQ, PTCZTffQ).**

Firstly, **PCDSeBT** simultaneously has a low-lying highest occupied molecular orbital (HOMO) energy level at −5.4 eV and a low band gap of 1.70 eV as required by the ideal polymers for BHJ PSCs. The remarkably high short-circuit current (*Jsc*) density, 11.7 mA/cm^2, was obtained in bulk heterojunction polymer solar cell based on **PCDSeBT**. The high J_{SC} value, along with a moderate fill factor (*FF*) of 45% and a high open-circuit voltage (V_{OC}) of 0.79 V, yields a power conversion.

Secondly, TCZT's polymers (**PTCZTBT**, **PTCZTfBT**, **PTCZTffBT, PTCZTTT**, **PTCZTPT**, **PTCZTQ**, **PTCZTfQ, PTCZTffQ)** comprising a S- and N-containing heteroarene, i.e, *N*-9′-heptadecanyldithieno[2,3-*b*;7,6-*b*]carbazole expected to have high hole mobility were gained by Stille coupling reaction between TCZT and benzothiadiazole/thienothiophene/thienopyrroldione/ quinoxaline derivatives with $Pd_2(dba)_3$/P(*o*-tol)$_3$ as catalyst in the yield of 57.8−91.8%.

Lastly, the **bis-PCBM dyad** has a higher LUMO level and stronger absorption than PCBM, which should potentially be a highly helpful for minimizing the energy loss in the electron transfer from the donor to the acceptor material as well as increasing current generation in BHJ solar cells.

Manuscript

International

(1) B. Kim, R. K. Cheedarala, Y. Kim, G. H. Kim, S. Cho, J. Lee, J. Kim, J. Y. Kim, C. Yang* "Field-effect Transistors and Photovoltaic Cell using Ladder-type Heteroacene Polymers bearing Carbazole and Thiophene ring units" KJF international conference on organic materials for electronics and photonics, September 15−18, Gyeoungju, Korea (2011).

Domestic

(1) B. Kim, H. Yeom, M. Yun, J. Y. Kim,* C. Yang* "Replacing thiophene with selenophene in PCDTBT to lower LUMO for efficient polymer solar cells," Ann. Meeting of the Polymer Society of Korea, **37** (2), October. 11−12 (2012).

(2) B. Kim, G. Kim, C. Yang* "Synthesis of Modified PCBM bisadduct Containing 4-nitro-α-cyanostilbene moiety," Ann. Meeting of the Polymer Society of Korea, **37** (1), April. 12−13 (2012).

(3) B. Kim, J. H. Seo, G. Kim, Y. Kim, J. Lee, J. Kim, Yang* "Genesis of [5,6]-Open Regioisomer via Direct Benzyne-C_{60} Cycloaddition" Ann. Meeting of the Polymer Society of Korea, **36** (1), April. 7−8 (2011).

Acknowledgements

UNIST 에서 석사학위를 받게 되어 기쁩니다. 처음 UNIST 에 왔을 때의 기분이 생생한데 벌써 2 년이 흘러 졸업 할 날이 왔습니다.

그 동안, 많이 부족한 저를 잘 가르쳐 주시고 이끌어 주신 양창덕 교수님께 정말 감사 드립니다. 함께 실험하고 생활했던 종기 오빠, 경식이 오빠, 규철이 오빠, gitish, chen 에게도 감사의 마음을 전하고 싶습니다. 조금 더 많은 시간을 보냈으면 좋을 것 같다는 아쉬움도 남지만, 각자의 길에서 열심히 해 나중에는 더 좋은 모습으로 볼 수 있으면 좋겠습니다. 1 년동안 모자란 친구를 엄마처럼 잘 챙겨준 현주와 경주에게도 감사 드립니다. 그 밖에도 UNIST 에 와서 만난 친구, 언니, 오빠들에게도 감사 드립니다.

마지막으로, 늘 든든한 후원자가 되어주고 마음의 안식처가 되어주는 우리 가족 아빠, 엄마, 남훈이 오빠, 광일이 오빠 모두 정말 감사하고 사랑합니다!